GEOPHYSICS, VOL. 73, NO. 3 (MAY-JUNE 2008); P. F115–F120, 12 FIGS.
10.1190/1.2904984

Annual Meeting Selection

Conductivity-depth imaging of helicopter-borne TEM data based on a pseudolayer half-space model

Haoping Huang[1] and Jonathan Rudd[2]

ABSTRACT

Helicopter-borne time-domain electromagnetic (HTEM) systems with a concentric horizontal coil configuration have been used increasingly in mineral exploration. Conductivity-depth imaging (CDI) is a useful tool for mapping the distribution of geologic conductivity and for identifying conductive targets. A CDI algorithm for HTEM systems with a concentric coil configuration is developed based on the pseudolayer half-space model. Primary advantages of this model are immunity to altimeter errors and better resolution of conductive layers than other half-space models. Effective depth is derived empirically from the diffusion depth and apparent thickness of the pseudolayer. A table lookup procedure is established based on the analytic solution of a half-space model to speed up processing. This efficiency makes generation of real-time conductivity-depth images possible. Tests on synthetic data demonstrate that the pseudolayer conductivity-depth-imaging algorithm maps a wider range of conductivities and does a better job of resolving highly conductive layers, compared with that of the homogeneous half-space model. Effective depths are close to true depths in many circumstances. Field examples show stable and geologically meaningful conductivity-depth images.

INTRODUCTION

Helicopter-borne time-domain electromagnetic (HTEM) systems with a concentric horizontal coil configuration now dominate the airborne electromagnetic industry and are used in mineral exploration, hydrologic projects, and oil and gas programs. In such applications, conductivity-depth imaging (CDI) of data has proven useful for the distribution of geologic conductivity and for identifying conductive layers within a variably conductive host geology. This approximate technique for interpreting EM data is based on the direct transformation of observed EM data to apparent conductivity and depth. Compared with true inversion methods (e.g., Huang and Palacky, 1991; Chen and Raiche, 1998; Ellis, 1998), CDI algorithms are very efficient because techniques do not require an initial model definition and iterative computations.

There are many techniques for deriving fast conductivity-depth sections from time-domain electromagnetic (TEM) data. The Maxwell receding image concept is commonly used for deriving conductivity from a predicted depth for an image source (e.g., Macnae and Lamontagne, 1987; Nekut, 1987; Macnae et al., 1998). Approximate imaging schemes based on the depth of the maximum current or maximum sensitivity to a layer in a half-space also have been developed (e.g., Eaton and Hohmann, 1989; Fullagar, 1989; Fullagar and Reid, 1992; Smith et al., 1994). Some researchers focused on how to accomplish deconvolutions or decompositions that take into account an arbitrary waveform to estimate the step response of the earth from off-time TEM measurements (e.g., Macnae et al., 1991; Wolfgram and Karlik, 1995; Chen and Macnae, 1998; Eaton, 1998; Stolz and Macnae, 1998). Thin-sheet approaches developed for TEM data also have been used to compute conductance and depth, which can be differentiated into a conductivity-depth section (Macnae et al., 1991; Liu and Asten, 1993; Tartaras et al., 2000). A modification of this method has been introduced to add the possibility of recovering magnetic properties of the geology (Zhdanov and Pavlov, 2001). Still further development of this technique has involved the application of the localized S-inversion (Zhdanov et al., 2002).

Apparent conductivity is typically obtained by transformation of the measured EM response and aircraft altimeter data assuming a half-space model. Techniques were developed by Fraser (1978) for

Presented at the 76th Annual International Meeting, SEG. Manuscript received by the Editor 22 May 2007; revised manuscript received 4 September 2007; published online 1 May 2008.
[1]Geo-EM, LLC, Raleigh, North Carolina, U.S.A. E-Mail: haoping_huang@hotmail.com
[2]Aeroquest, Ltd., Mississauga, Ontario, Canada

frequency-domain systems and by Dyck et al. (1974) and Palacky (1981) for time-domain systems. Figure 1 shows two half-space models in which Figure 1a is termed *homogeneous half-space model* and Figure 1b *pseudolayer half-space model* (Fraser, 1978). The upper (pseudo) layer of the pseudolayer half-space model of Figure 1b is merely an artifice to account for the difference between computed sensor-source distance h and measured sensor altitude a. Measured sensor altitude is determined from the radar or laser altimeter. Any error in the altimeter reading, e.g., an error caused by a forest canopy, falls into the computed sensor-source height and therefore does not corrupt the computed conductivity. In frequency-domain airborne EM methods, the pseudolayer half-space is the model of choice for displaying apparent resistivity in both plan (Fraser, 1990) and section (Sengpiel, 1988), partly because of this immunity to altimeter errors. Another merit of the pseudolayer model is better resolution of conductive layers. Furthermore, derived apparent conductivity spans a larger range. These aspects of the model tend to make conductive bedrock layers more recognizable than when the homogeneous half-space model is employed (Fraser, 1978, 1990).

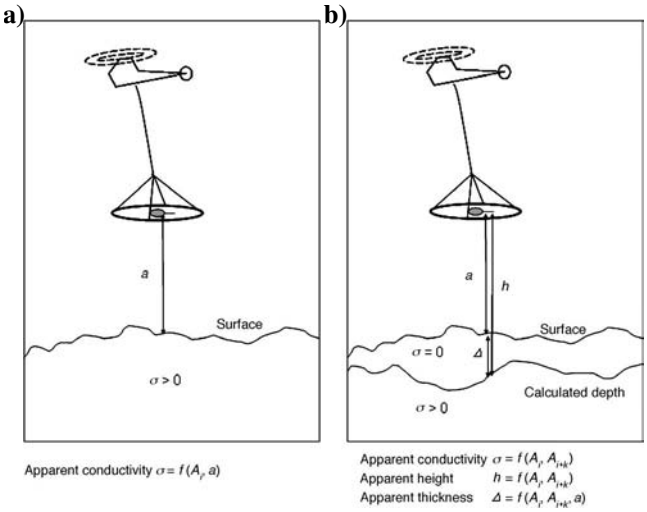

Figure 1. Sketch of the HTEM system and half-space models. Transmitter consists of a large loop towed by a helicopter with receivers located at the center of the transmitter loop. (a) Homogeneous half-space model in which the top of the half-space coincides with earth's surface, as defined by radar or laser altimeter. (b) Pseudolayer half-space model in which the top of the half-space is defined numerically by output parameter h. The pseudolayer half-space model is equivalent to a two-layer case in which the upper layer is of zero conductivity. Thickness Δ is the difference between interpreted height h and bird altitude a as obtained from the altimeter.

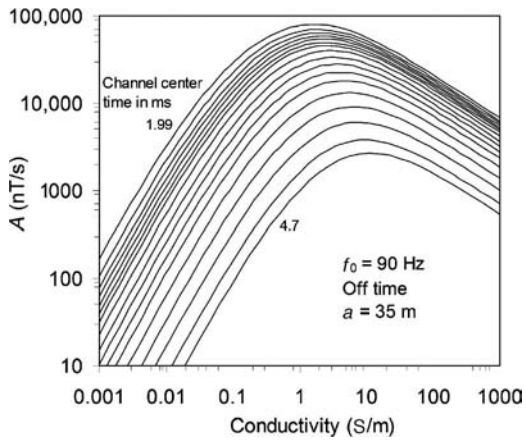

Figure 2. Seventeen channel off-time responses to a homogeneous half-space for 12-m bird at a height of 35 m. Base frequency f_0 = 90 Hz.

Conductivity transformation of TEM data based on pseudolayer half-space was developed by Palacky (1981), even if he did not specify the point. Based on both Fraser's and Palacky's work, Huang et al. (1983) portrayed explicitly the pseudolayer technique for airborne TEM systems. However, techniques reported in the early 1980s yielded a single conductivity from all channel data and were used for conductivity mapping rather than for depth sounding.

We present an approach to CDI using a pseudolayer half-space model. The concept of the effective depth is used. The new algorithm, as applied to HTEM data, is tested on synthetic and field data with encouraging results.

AEROTEM SYSTEMS

The original concept of a coincident coil HTEM system was pioneered by Aerodat scientists in the early 1980s under Wally Bokyo's guidance. Since then, Aeroquest has refined the system design into an effective and fieldworthy exploration tool that is optimized to provide the maximum amount of information on a target conductor. The transmitter consists of a large loop towed by a helicopter with receivers located at the center of the transmitter loop. Diameter of the transmitter loop can be 5 m, 9 m, or 12 m. The transmitter waveform is a bipolar symmetric triangular pulse which can be operated at 150, 90, and 30 Hz with a 30–50% duty cycle. The transmitter moment is 4×10^4 Am^2 for the 5-m system and 2.3×10^5 Am^2 for the 12-m system. Vertical and inline horizontal components of induced voltage of the secondary magnetic fields are measured during transmitter on time and off time. There are 16 on-time channels plus 17 off-time channels for both components. Finite transmitter turnoff time might affect TEM data collected at times shortly after transmitter turnoff when transmitter turnoff time is large (Fitterman and Anderson, 1984). AeroTEM systems allow sufficient time between transmitter turnoff and first time-off data sampling to avoid the effects of transmitter turnoff. Strengths of AeroTEM systems include high spatial resolution, broadband response, source geometry discrimination, and depth of investigation.

METHOD

A sketch of the HTEM system and half-space models is shown in Figure 1. The transmitter consists of the large loop towed by a helicopter and the horizontal and vertical component receiver coils located at the center of the transmitter loop. For concentric transmitting and receiving coils, the half-space response in the frequency domain can be found in Ward and Hohmann (1988). This response can be Fourier-transformed to the time-domain. Figure 2 depicts the off-time response A to a half-space as a function of conductivity σ. The response for each channel, given in nT/s, increases with increasing conductivity at low conductivities, reaches a peak at moderate conductivity (about 1 S/m), and then decreases as σ continues to increase.

Figure 2 shows that conductivity cannot be determined uniquely from a single channel of data but can be derived from any two chan-

nels. Assuming decay curves can be approximated as a piecewise exponential function of time, we can calculate the time constant, τ_i, from two channels as

$$\tau_i = \frac{t_{i+k} - t_i}{\ln\left(\frac{A_i}{A_{i+k}}\right)}, \quad (1)$$

where t_i and A_i are the center time and measured response in nT/s for the ith channel, respectively, and k (≥ 1) is the channel interval used to calculate τ_i, which can be 1 for high-quality data and as much as 4 for low-quality data.

Then we define the amplitude α_i to be

$$\alpha_i = (A_i^2 + A_{i+k}^2)^{1/2}. \quad (2)$$

Apparent conductivity σ_a and apparent bird height h can be computed from a pair of τ_i and α_i. Apparent thickness Δ of the pseudolayer (= depth to top of half-space) can be calculated from h and measured bird altitude a, i.e., $\Delta = h - a$. If N channels of data are available, N-k apparent conductivities and apparent thicknesses can be computed.

In practice, we create a lookup table to compute σ and h based on analytic solutions to speed up the process. This procedure is understood easily by using a graphical presentation shown in Figure 3. A diagram is used to yield a unique σ and h from each pair of τ_i and α_i. For measured data, we calculate τ_i and α_i from channel i and channel $i + k$. These pairs, τ_i and α_i, then locate a point on a corresponding diagram such as Figure 3, which is one of the N-k diagrams. The point determines conductivity σ and height h. Solutions are interpolated in which the location does not fall directly on conductivity-altitude curves. If the earth is truly homogeneous, the conductivity obtained from Figure 3 is equal to the true conductivity σ. When it is not homogeneous, the solution is an apparent conductivity σ_a.

Conductivity σ_i of channel i will be associated with an effective depth d_i that we determine next. We begin with the time-domain diffusion depth, which is proportional to the square root of sampling time t_i and inverse conductivity σ_i. Thus, we write

$$\delta_i = \left(\frac{2t_i}{\sigma_i \mu_0}\right)^{1/2}, \quad (3)$$

where μ_0 is the magnetic permeability of free space. Because the pseudolayer model is used, effective depth is related to apparent thickness and can be written generally as

$$d_i = f(\delta_i, \Delta_i) \quad (4)$$

(Huang and Fraser, 1996), where the function itself is determined empirically based on experimentation with synthetic data. Figure 4 provides a graphic presentation of our choice of the effective depth as a function of δ_i and Δ_i.

Tests on synthetic data

We have compared output of the homogeneous half-space and pseudolayer half-space algorithms for a variety of layered earth examples. We refer to apparent conductivities obtained from the homogeneous half-space model as homogeneous conductivity and those from the pseudolayer model as pseudolayer conductivity. Algorithms were tested on synthetic data obtained from a series of homogeneous half-space models in which testing yielded output conductivities from the homogeneous algorithm and conductivities and pseudolayer thicknesses from the pseudolayer algorithm. Conductivity returned for each channel pair yielded errors generally less than 0.1%, and computed pseudolayer thicknesses were all 0 ± 0.1 m. Having established the efficacy of algorithms for a half-space, we now apply them to a variety of multilayer earth synthetic data to determine their usefulness in yielding CDIs that are reflective of layering in the earth.

In the following examples, synthetic data were computed using AeroTEM 5-m system data and parameters. Width of the transmitted pulse is 1.1 ms, and 17 off-time data channels were used for soundings with $k = 3$ for pseudolayer conductivity. Because model studies were conducted using layered-earth models, only the vertical component is considered.

We first examine two two-layer cases, one of which has a resistive upper layer (Figure 5a) and the other a conductive upper layer (Figure 5b). In both cases, the upper layer is 100 m thick. The first model (Figure 5a) has a surface-layer conductivity of 10 mS/m and basement conductivity of 100 mS/m. The second model (Figure 5b) has a surface-layer conductivity of 100 mS/m and basement conductivity of 10 mS/m. Apparent conductivities are computed using the ho-

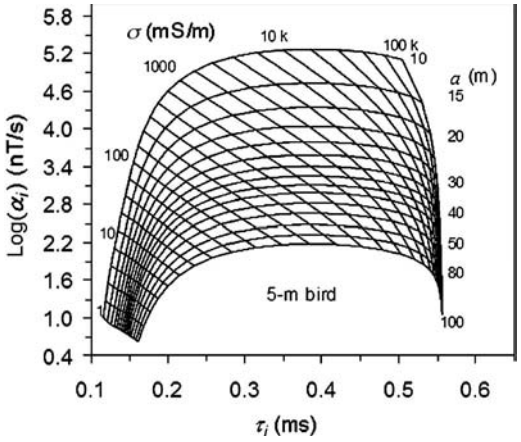

Figure 3. Diagram of time constant τ_i and amplitude α_i (in logarithmic space) of half-space model for two time-off channels.

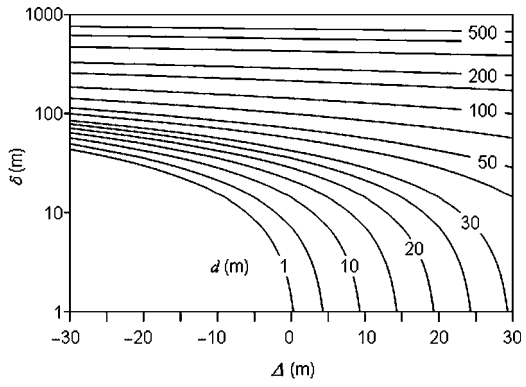

Figure 4. The effective depth computed from an empirical as a function of δ and Δ.

mogeneous and pseudolayer models. Analogous to findings in the frequency-domain case, conductive targets at depth are imaged better by using the pseudolayer method, whereas the homogeneous half-space method tends to represent near-surface conductivity better (Fraser, 1978, 1990). Figure 5a shows that pseudolayer conductivity is closer to the true value of the conductive basement than homogeneous conductivity is. In Figure 5b, the presence of the resistive basement is indicated somewhat by pseudolayer conductivity, whereas it is indicated very poorly by homogeneous conductivity.

We now examine the response to three-layer cases. Figure 6a displays a conductive thin layer (200 mS/m, 20 m thick) underlying a moderately resistive cover (20 mS/m, 100 m thick) with a resistive basement (2 mS/m). Figure 6b illustrates a 20-m-thick resistive layer (5 mS/m) sandwiched in a conductive host (50 mS/m) at 100-m depth. Pseudolayer conductivity, shown in Figure 6a, clearly indicates a three-layer earth, whereas the homogeneous conductivity algorithm fails to indicate the resistive basement. Pseudolayer conductivity is not significantly superior to homogeneous conductivity in the case of a resistive middle layer (Figure 6b), illustrating the difficulty of detecting thin resistive layers with EM.

Figure 7 depicts results from a four-layer earth with conductivities 100-2-500-2 mS/m reflecting conductive overburden on a resistive

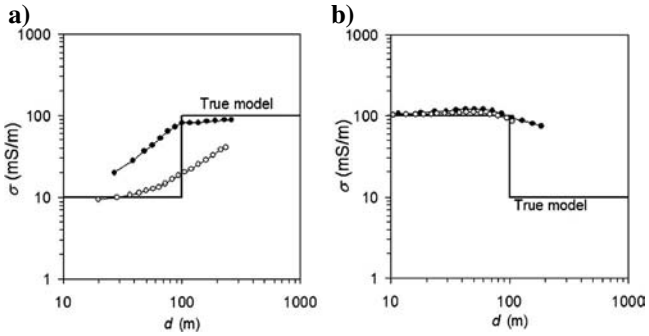

Figure 5. Conductivity-depth diagrams for two-layer models. First layer thickness is 100 m. Layer conductivities are (a) 10 and 100 mS/m and (b) 100 and 10 mS/m. The straight lines are true model conductivities, the curves with solid circles are pseudolayer conductivities, and the curves with open circles are homogeneous conductivities.

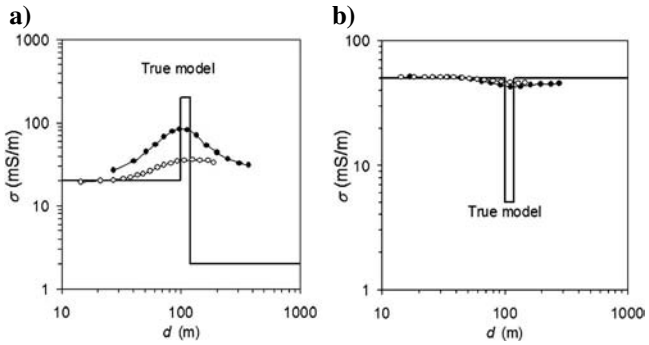

Figure 6. Conductivity-depth diagrams for two three-layer models. Layer conductivities from the surface to depth are (a) 20, 200, and 2 mS/m and (b) 50, 5, and 50 mS/m. The first layer is 100 m thick, and the second layer is 20 m thick. The straight lines are true model conductivities, the curves with solid circles are pseudolayer conductivities, and the curves with open circles are homogeneous conductivities.

host containing a conductive target layer. The thin conductive layer (10 m) is at 100-m and 200-m depths in Figure 7a and b, respectively. Curves for both the homogeneous and pseudolayer algorithms indicate qualitatively that a four-layer earth exists when the thin conducting layer is shallower (Figure 7a). When the depth to the thin layer is increased to 200 m, we cannot detect the resistive basement from homogeneous conductivity. However, the pseudolayer curve rapidly follows sharp changes in conductivity at layer interfaces, thereby indicating existence of resistive material below the conductor.

We now simulate an isolated conducting lens-shaped object in a moderately resistive host. Conductivity of the lens-shaped object is 200 mS/m, and thickness at its center is 25 m. The lens is located at the center of the profile at a 180-m depth in a 20 mS/m host. Synthetic data are computed from a series of 1D models to form a data profile shown in Figure 8a. Responses over the object are lower than those of the background for early-time channels because of over-

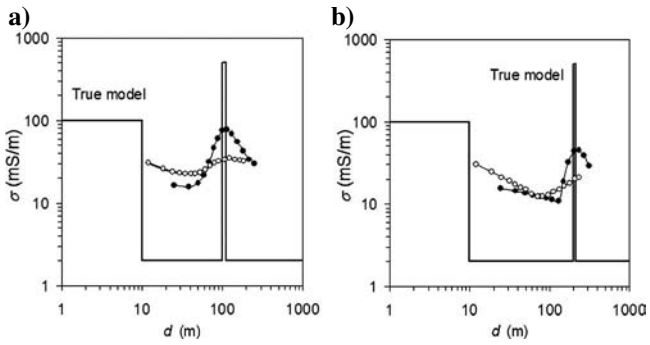

Figure 7. Conductivity-depth diagrams for two four-layer models. Layer conductivities from the surface to depth are 100, 2, 500, and 2 mS/m. The first layer is 10 m thick. The thin conductive third layer is 10 m thick. Depth to this layer is (a) 100 m and (b) 200 m, respectively. The straight lines are true model conductivities, the curves with solid circles are pseudolayer conductivities, and the curves with open circles are homogeneous conductivities.

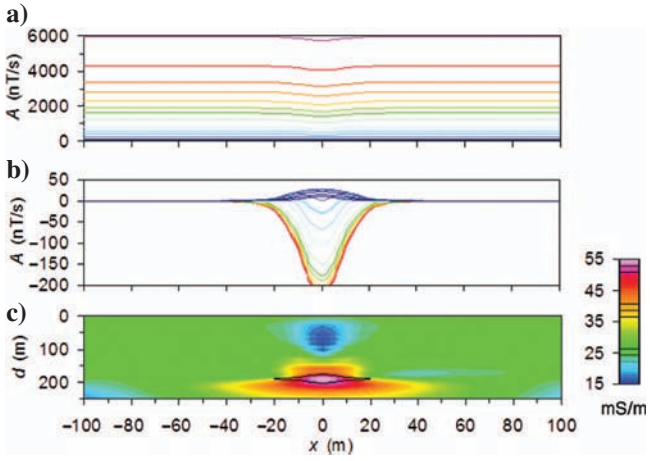

Figure 8. A conductive lenslike object (200 mS/m) in a moderately resistive host (20 mS/m). Top of lens is 180 m deep. Maximum thickness of lens is 25 m. (a) Synthetic responses computed from a series of 1D models. (b) Synthetic response with background response removed. Warm colors indicate early-time channels and cool colors late-time channels. (c) Imaged conductivity-depth section with lens outlined.

shoot/undershoot effects which commonly are seen in electrical soundings. A positive anomaly is shown on later-time channels. These can be seen clearly by removing the background response, as presented in Figure 8b. We added 5% random noise to the synthetic data and then computed pseudolayer conductivities and depths. The resulting conductivity-depth image is illustrated in Figure 8c, with the lens-shaped object outlined in black.

Finally, we consider a resistive lens-shaped object (5 mS/m) in a moderately conductive host (20 mS/m). The depth to the top of the lens is 50 m, and thickness at the center of the lens is 80 m. Figure 9 shows synthetic responses with and without background and the conductivity-depth section. Responses above the lens are lower than that of the background for all time channels because of the resistive object at depth.

Field examples

Data for the following two field examples were collected using an AeroTEM system. The first example is from an area where a variable layer of conductive overburden occurs over a resistive geology. Figure 10 shows off-time data from a 23-km line and resulting CDI section. Much of the line has a high-amplitude, rapidly decaying response typical of a thin conductive surface layer. This response appears to be modeled correctly in CDI as a near-surface conductive layer. This data set, which comprises more than 10,000 data points, took only a few seconds to process for apparent conductivities and depths.

The second AeroTEM field example is from the oil sands area in northern Alberta, Canada. The survey was flown with 250-m line spacing in an east-west orientation. CDI sections were computed for all lines, and a conductivity volume was constructed by interpolating results from section to section across the survey area. Figure 11 depicts the CDI volume. The more conductive zones are shown in cooler colors, and resistive geology is shown in warmer colors.

Conductive shales of the Clearwater Formation overlie McMurray Formation sandstone (reservoir rock). Both units have a shallow easterly dip across the survey area. The top edge of the Clearwater Formation can be seen in the far northwestern corner of the block where the resistive McMurray Formation is at surface. Conductivity

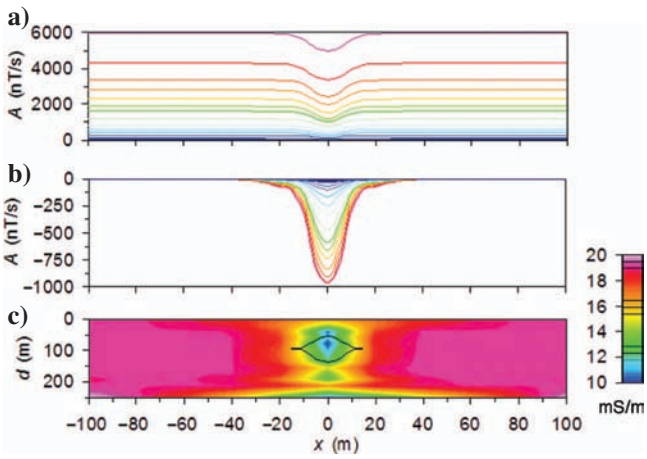

Figure 9. A resistive lenslike object (5 mS/m) in a moderately conductive host (20 mS/m). Top of lens is 50 m deep. Lens thickness is 80 m. (a) Synthetic responses computed from a series of 1D models. (b) Synthetic response with background response removed. Warm colors indicate early-time channels and cool colors late-time channels. (c) Imaged conductivity-depth section with lens outlined.

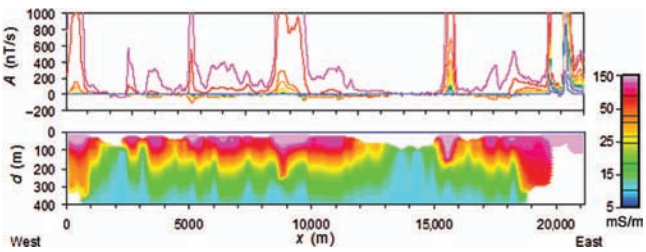

Figure 10. HTEM data obtained from a resistive area and CDI section. Warm colors indicate early-time channels, and cool colors indicate late-time channels.

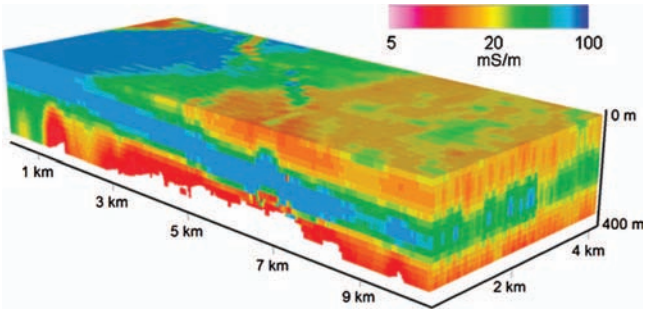

Figure 11. CDI volume computed from AeroTEM data obtained from an oil-sands area in Alberta, Canada.

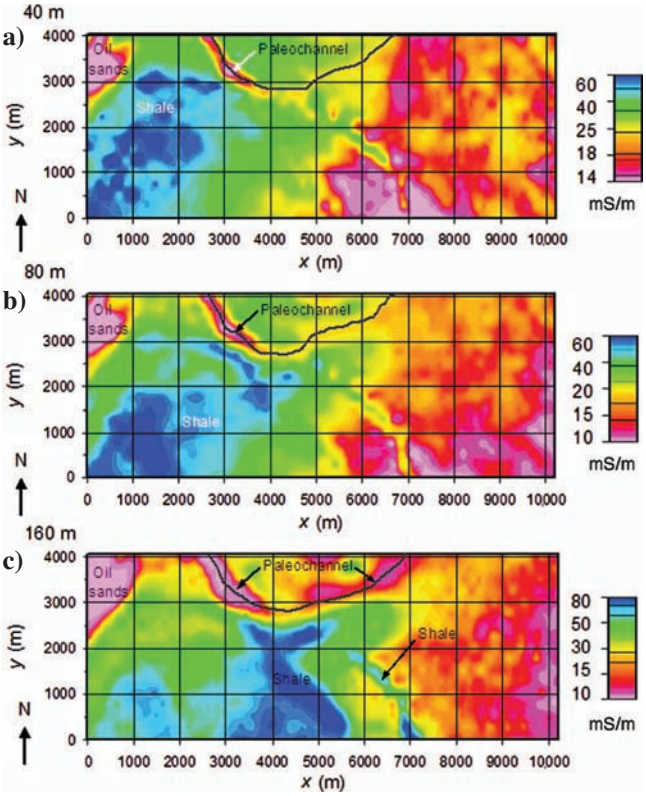

Figure 12. Three apparent conductivity-depth slices at (a) 40 m, (b) 80 m, and (c) 160 m based on CDI results.

imaging has identified a variably conductive near-surface layer in the eastern half of the survey area. Resistive portions of this layer correlate well with known aggregate accumulations. A paleochannel can be seen clearly, based on morphology in the northern portion of the survey block. CDI indicates that the channel is filled with relatively resistive sediment.

Three depth-slice plan images at depths of 40 m, 80 m, and 160 m are shown in Figure 12. Conductivity maps, which can be produced for any depth from CDI results, are an effective way of visualizing conductive layers and features in plan view at various depths. The conductive shale unit shown in cooler colors dips gently to the east. Resistive channels clearly stand out in northwestern and northern areas (x = 2500–7000 m and y = 2900–4000 m), probably cutting entirely through the shale unit in the northwest. More resistive areas which overlie shales are likely to reflect potential aggregate sources. The resistive area in and around x = 6200 m and y = 500 m is a known accumulation of approximately 120 m of sandy overburden. When combined with even sparse drilling information, HTEM data are very useful in mapping various geologic features in this environment.

CONCLUSIONS

An algorithm has been developed for transforming HTEM data to apparent conductivity and effective depth based on the pseudolayer half-space model. Compared with the homogeneous half-space model, there are two advantages of the pseudolayer technique — immunity to altimeter errors and better identification and resolution of conductive layers. A table lookup procedure is issued based on the analytic solution to the pseudolayer half-space model to speed up processing. This makes real-time processing of conductivity-depth images possible. Tests on synthetic data demonstrate that pseudolayer conductivity is sensitive to a wider range of conductivities and does a better job of resolving good conductors. The effective depth derived empirically from diffusion depth and apparent thickness of the pseudolayer is close to true depth in a wide range of circumstances. Field examples show stable and geologically meaningful conductivity-depth sections.

ACKNOWLEDGMENTS

The authors thank Associated Mining Consultants Ltd., Calgary, Alberta, Canada, for valuable contributions to this paper. Appreciation is expressed to David Fitterman and Douglas Fraser for constructive reviews that greatly helped improve this paper. In addition, appreciation is expressed to editors and anonymous reviewers for their valuable comments and suggestions.

REFERENCES

Chen, J., and J. C. Macnae, 1998, Automatic estimation of EM parameters in tau-domain: Exploration Geophysics, **29**, 170–174.

Chen, J., and A. Raiche, 1998, Inverting AEM data using a damped eigenparameter method: Exploration Geophysics, **29**, 128–132.

Dyck, A. V., A. Becker, and L. S. Collett, 1974, Surficial conductivity mapping with the airborne INPUT system: Canadian Institute of Mining and Metallurgical Bulletin, 67, 104–109.

Eaton, P. A., 1998, Application of an improved technique for interpreting transient electromagnetic data: Exploration Geophysics, **29**, 175–183.

Eaton, P. A., and G. W. Hohmann, 1989, A rapid inversion technique for transient electromagnetic soundings: Physics of the Earth and Planetary Interiors, **53**, 384–404.

Ellis, R. G., 1998, Inversion of airborne electromagnetic data: Exploration Geophysics, **29**, 121–127.

Fitterman, D. V., and W. L. Anderson, 1984, Effect of transmitter turnoff characteristics on transient soundings: 54th Annual International Meeting, SEG, Expanded Abstracts, 69–71.

Fraser, D. C., 1978, Resistivity mapping with an airborne multicoil electromagnetic system: Geophysics, **43**, 144–172.

———, 1990, Layered-earth resistivity mapping, *in* D. V. Fitterman, ed., Developments and applications of modern airborne electromagnetic surveys: United States Geological Survey Bulletin, 1925, 33–41.

Fullagar, P. K., 1989, Generation of conductivity-depth pseudo-sections for coincident loop and in-loop TEM data: Exploration Geophysics, **20**, 43–45.

Fullagar, P. K., and J. E. Reid, 1992, Conductivity-depth transformations of fixed loop TEM data: Exploration Geophysics, **23**, 515–520.

Huang, H., and D. C. Fraser, 1996, The differential parameter method for multifrequency airborne resistivity mapping: Geophysics, **61**, 100–109.

Huang, H., and G. J. Palacky, 1991, Damped least-squares inversion of time domain airborne electromagnetic data based on singular value decomposition: Geophysical Prospecting, **39**, 827–844.

Huang, H., H. Xi, Y. Wang, D. Zhu, and H. Piao, 1983, Transformation of the time-domain airborne electromagnetic response to apparent resistivity and its application in geological mapping: Journal of Changchun College of Geology, **3**, 135–144.

Liu, G., and M. Asten, 1993, Conductance-depth imaging of airborne TEM data: Exploration Geophysics, **24**, 655–662.

Macnae, J. C., A. King, N. Stolz, A. Osmakoff, and A. Blaha, 1998, Fast AEM data processing and inversion: Exploration Geophysics, **29**, 163–169.

Macnae, J., and Y. Lamontagne, 1987, Imaging quasi-layered conductive structures by simple processing of transient electromagnetic data: Geophysics, **52**, 545–554.

Macnae, J. C., R. Smith, B. D. Polzer, Y. Lamontagne, and P. S. Klinkert, 1991, Conductivity-depth imaging of airborne electromagnetic step-response data: Geophysics, **56**, 102–114.

Nekut, A. G., 1987, Direct inversion of time-domain electromagnetic data: Geophysics, **52**, 1431–1435.

Palacky, G. J., 1981, The airborne electromagnetic method as a tool of geological mapping: Geophysical Prospecting, **29**, 60–88.

Sengpiel, K. P., 1988, Approximate inversion of airborne EM data from a multilayered ground: Geophysical Prospecting, **36**, 446–459.

Smith, R. S., R. N. Edwards, and G. Buselli, 1994, Automatic technique for presentation of coincident-loop, impulse-response, transient, electromagnetic data: Geophysics, **59**, 1542–1550.

Stolz, E. M., and J. C. Macnae, 1998, Evaluating EM waveforms by singular-value decomposition of exponential basis functions: Geophysics, **63**, 64–74.

Tartaras, E., M. S. Zhdanov, K. Wada, A. Saito, and T. Hara, 2000, Fast imaging of TDEM data based on S-inversion: Journal of Applied Geophysics, **43**, 15–32.

Ward, S. H., and G. W. Hohmann, 1988, Electromagnetic theory for geophysical applications, *in* M. N. Nabighian, ed., Electromagnetic methods in applied geophysics, v., 1, Theory: SEG, 130–311.

Wolfgram, P., and G. Karlik, 1995, Conductivity-depth transform of GEOTEM data: Exploration Geophysics, **26**, 179–185.

Zhdanov, M. S., and D. A. Pavlov, 2001, Analysis and interpretation of anomalous conductivity and magnetic permeability effects in time domain electromagnetic data: Part II: Sμ-inversion: Journal of Applied Geophysics, **46**, 235–248.

Zhdanov, M. S., D. A. Pavlov, and R. Ellis, 2002, Localized S-inversion of time domain electromagnetic data: Geophysics, **67**, 1115–1125.

Report on a Helicopter-Borne AeroTEM System Electromagnetic & Magnetic Survey

Aeroquest Job # 10-007

Rabbit Mine Property

Princeton, B.C., Canada
NTS 092H10
For

Max Investments Inc.

On behalf of Discovery Ventures Inc.

by

7687 Bath Road,
Mississauga, ON, L4T 3T1
Tel: (905) 672-9129
Fax: (905) 672-7083
www.aeroquest.ca

Report date: February 2010

Report on a Helicopter-Borne AeroTEM System Electromagnetic & Magnetic Survey

Aeroquest Job # 10-007

Rabbitt Mine Property

Princeton, B.C., Canada
NTS 092H10

For

Max Investments Inc.

On behalf of Discovery Ventures Inc.

3750 West 49th Avenue
Vancouver, BC, Canada
V6N-3TB

by

AEROQUEST

7687 Bath Road,
Mississauga, ON, L4T 3T1
Tel: (905) 672-9129
Fax: (905) 672-7083
www.aeroquest.ca

Report date: February 2010

TABLE OF CONTENTS

TABLE OF CONTENTS i
LIST OF FIGURES 2
LIST OF MAPS (1:10,000) 2
1. INTRODUCTION 3
2. SURVEY AREA 3
3. SURVEY SPECIFICATIONS AND PROCEDURES 4
3.1. Navigation 4
3.2. System Drift 4
3.3. Field QA/QC Procedures 4
4. AIRCRAFT AND EQUIPMENT 5
4.1. Aircraft 5
4.2. Magnetometer 6
4.3. Electromagnetic System 6
4.4. AeroDAS Acquisition System 7
4.5. Magnetometer Base Station 8
4.6. Radar Altimeter 8
4.7. Video Tracking and Recording System 9
4.8. GPS Navigation System 9
4.9. Digital Acquisition System 9
5. PERSONNEL 10
6. DELIVERABLES 10
6.1. Hardcopy Deliverables 10
6.2. Digital Deliverables 10
6.2.1. Final Database of Survey Data (.GDB) 10
6.2.2. Geosoft Grid files (.GRD) 10
6.2.3. Digital Versions of Final Maps (.MAP, .PDF) 11
6.2.4. Google Earth Files (.kmz) 11
6.2.5. Free Viewing Software (.EXE) 11
6.2.6. Digital Copy of this Document (.PDF) 11
7. DATA PROCESSING AND PRESENTATION 11
7.1. Base Map 11
7.2. Flight Path & Terrain Clearance 12
7.3. Electromagnetic Data 12
7.4. Magnetic Data 13
8. General Comments 13
8.1. Magnetic Response 13
8.2. Apparent Resistivity 13
8.3. EM Anomalies 13
APPENDIX 1: Survey Boundaries 16

APPENDIX 2: Description of Database Fields 17
APPENDIX 3: AeroTEM Anomaly Listing 18
APPENDIX 4: AeroTEM Design Considerations 22
APPENDIX 5: AeroTEM Instrumentation Specification Sheet 28

LIST OF FIGURES

Figure 1. Rabbitt Mine Property with flight path, overlain on shaded topography..... 3
Figure 2. Helicopter registration number C-GLOV 5
Figure 3. The magnetometer bird (A) and AeroTEM III EM bird (B)..... 6
Figure 4. Schematic of Transmitter and Receiver waveforms..... 7
Figure 5. AeroTEM III Instrument Rack..... 7
Figure 6. Digital video camera typical mounting location. 9
Figure 7. AeroTEM response to a ‘thin’ vertical conductor. 14
Figure 8. AeroTEM response for a ‘thick’ vertical conductor..... 14
Figure 9. AeroTEM response over a ‘thin’ dipping conductor. 15

LIST OF MAPS (1:10,000)

- TMI –Total Magnetic Intensity (TMI) with line contours and EM anomaly symbols.
- Z1-OFF– AeroTEM Z1 Off-time with line contours, and EM anomaly symbols.
- EM – AeroTEM off-time profiles Z3 – Z13, and EM anomaly symbols.
- DTM – Digital Terrain Model with line contours, and EM anomaly symbols.
- RES – Early Off-time Resistivity, and EM anomaly symbols.

1. INTRODUCTION

This report describes a helicopter-borne geophysical survey carried out on behalf of Max Investments Inc. for Rabbit Mine Property, near Princeton, B.C.

The principal geophysical sensor is Aeroquest's exclusive AeroTEM III (Mike) time domain helicopter electromagnetic system which is employed in conjunction with a high-sensitivity caesium vapour magnetometer. Ancillary equipment includes a real-time differential GPS navigation system, radar altimeter, video recorder, and a base station magnetometer. Full-waveform streaming EM data is recorded at 36,000 samples per second. The streaming data comprise the transmitted waveform, and the X component and Z component of the resultant field at the receivers.

The total survey coverage is 401 line-km, of which 371 line-km fell within the defined project area (Appendix 1). The survey was made up of one block, flown at 50 metre line spacing and at 75º/345º flight direction (Table 1). The survey flying described in this report took place from December 7th - December 9th, 2009. This report describes the survey logistics, the data processing, presentation, and provides the specifications of the survey.

2. SURVEY AREA

The Project area is located in central B.C. The survey consisted of one block, Rabbit Mine Property and was located approximately 25 kilometres Northwest of Princeton, B.C. The base of survey operations was at Princeton, B.C.

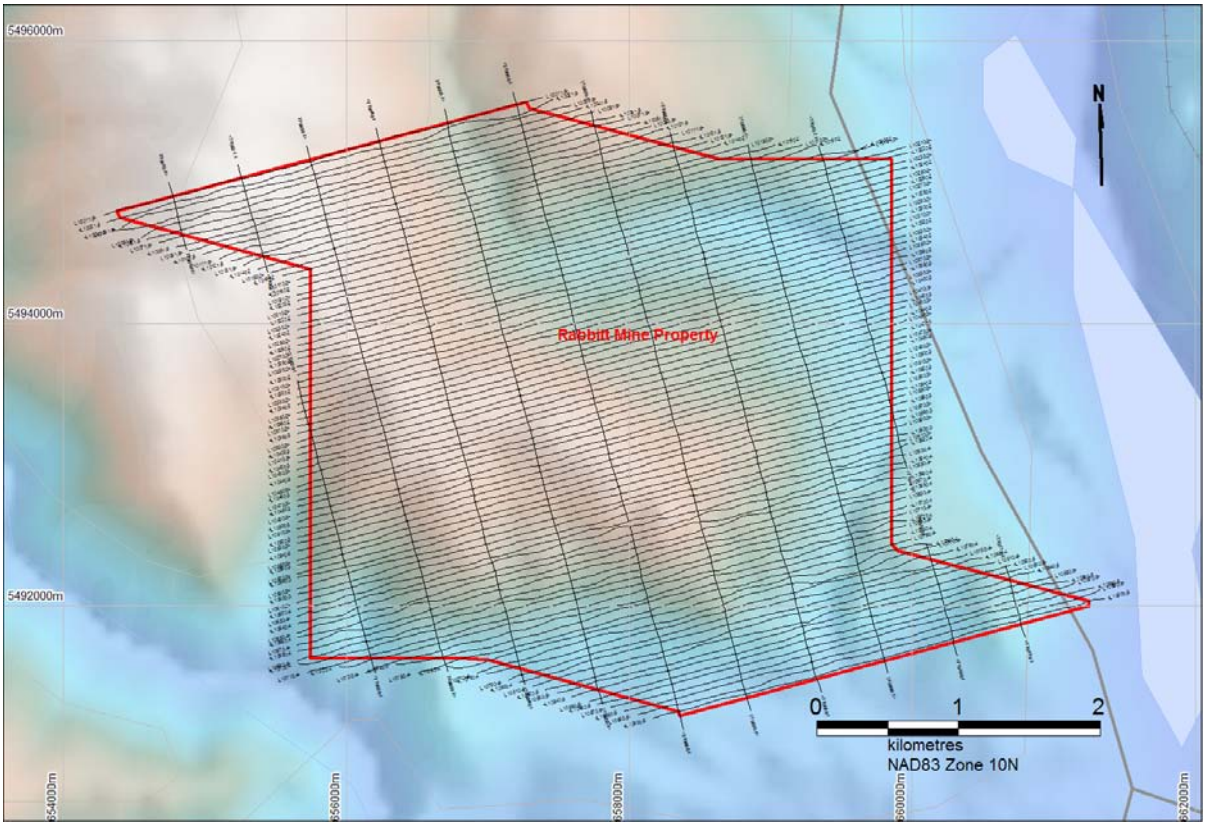

Figure 1. Rabbitt Mine Property with flight path, overlain on shaded topography

3. SURVEY SPECIFICATIONS AND PROCEDURES

The survey specifications are summarised in the following table:

Project Name	Line/Tie Spacing (metres)	Line Direction	Survey Coverage (line-km)	Date flown
Rabbit Mine Property	50/500	75º/345º	401	December 7th - December 9th, 2009

Table 1. Survey specifications summary

The survey coverage was calculated by summing the along-line distance of the survey lines and control (tie) lines as presented in the final Geosoft database. The survey was flown with a line spacing of 50 metres. The control (tie) lines were flown perpendicular to the survey lines with 500 metres, tie line spacing.

The nominal EM bird terrain clearance is 30 metres, but can be higher in more rugged terrain due to safety considerations and the capabilities of the aircraft. The magnetometer sensor is mounted in a smaller bird connected to the tow rope 30.5 metres above the EM bird and 18.3 metres below the helicopter (Figure 3). Nominal survey speed over relatively flat terrain is 75 km/hr and is generally lower in rougher terrain. Scan rates for ancillary data acquisition is 0.1 second for the magnetometer and altimeter, and 0.2 second for the GPS determined position. The EM data is acquired as a data stream at a sampling rate of 36,000 samples per second and is processed to generate final data at 10 samples per second. The 10 samples per second translate to a geophysical reading about every 1.5 to 2.5 metres along the flight path.

3.1. NAVIGATION

Navigation is carried out using a GPS receiver, an AGNAV2 system for navigation control, and an RMS DGR-33 data acquisition system which records the GPS coordinates. The x-y-z position of the aircraft, as reported by the GPS, is recorded at 0.2 second intervals. The system has a published accuracy of less than 3 metres. A recent static ground test of the Mid-Tech WAAS GPS yielded a standard deviation in x and y of less than 0.6 metres and for z less than 1.5 metres over a two-hour period.

3.2. SYSTEM DRIFT

Unlike frequency domain electromagnetic systems, the AeroTEM III system has negligible drift due to thermal expansion. The operator is responsible for ensuring the instrument is properly warmed up prior to departure and that the instruments are operated properly throughout the flight. The operator maintains a detailed flight log during the survey noting the times of the flight and any unusual geophysical or topographic features. Each flight included at least two high elevation 'background' checks. During the high elevation checks, an internal 5 second wide calibration pulse in all EM channels was generated in order to ensure that the gain of the system remained constant and within specifications.

3.3. FIELD QA/QC PROCEDURES

On return of the pilot and operator to the base, usually after each flight, the AeroDAS streaming EM data are carried on removable hard drives and Flashcards, respectively and transferred to the data processing work station. At the end of each day, the base station magnetometer data on FlashCard is retrieved from the base station unit.

Data verification and quality control includes a comparison of the acquired GPS data with the flight plan; verification and conversion of the RMS data to an ASCII format XYZ data file; verification of the base station magnetometer data and conversion to ASCII format XYZ data; and loading, processing and conversion of the steaming EM data from the removable hard drive. All data is then merged to an ASCII XYZ format file which is then imported to an Oasis database for further QA/QC and for the production of preliminary EM, magnetic contour, and flight path maps.

Survey lines which show excessive deviation from the intended flight path are re-flown. Any line or portion of a line on which the data quality did not meet the contract specification was noted and reflown.

4. AIRCRAFT AND EQUIPMENT

4.1. AIRCRAFT

A Eurocopter (Aerospatiale) SA 315B - registration C-GLOV was used as survey platform. The helicopter was owned and operated by Hi-Wood Helicopters Ltd. Installation of the geophysical and ancillary equipment was carried out by Aeroquest Limited personnel in conjunction with a licensed aircraft. The survey aircraft was flown at a nominal terrain clearance of 275 ft (82metres).

Figure 2. Helicopter registration number C-GLOV

4.2. MAGNETOMETER

The AeroTEM III airborne survey system employs the Geometrics G-823A caesium vapour magnetometer sensor installed in a two metre towed bird airfoil attached to the main tow line, 18.3 metres below the helicopter (Figure 3). The sensitivity of the magnetometer is 0.001 NanoTesla at a 0.1 second sampling rate. The nominal ground clearance of the magnetometer bird is 60.5 metres (198 ft.). The magnetic data is recorded at 10 Hz by the ADAS.

4.3. ELECTROMAGNETIC SYSTEM

The electromagnetic system is an Aeroquest AeroTEM III time domain towed-bird system (Figure 3). The current AeroTEM III transmitter dipole moment is 179 kNIA. The AeroTEM bird is towed 48.8 metres (160 ft) below the helicopter. More technical details of the system may be found in Appendix 5.

The wave-form is triangular with a symmetric transmitter on-time pulse of 1.10 ms and a base frequency of 90 Hz (Figure 4). The current alternates polarity every on-time pulse. During every Tx on-off cycle (180 per second), 200 contiguous channels of raw X and Z component (and a transmitter current monitor, itx) of the received waveform are measured. Each channel width is 27.78 microseconds starting at the beginning of the transmitter pulse. This 200 channel data is referred to as the raw streaming data. The AeroTEM system has one separate EM data recording stream, the newly designed AeroDAS system which records the full waveform (Figure 5).

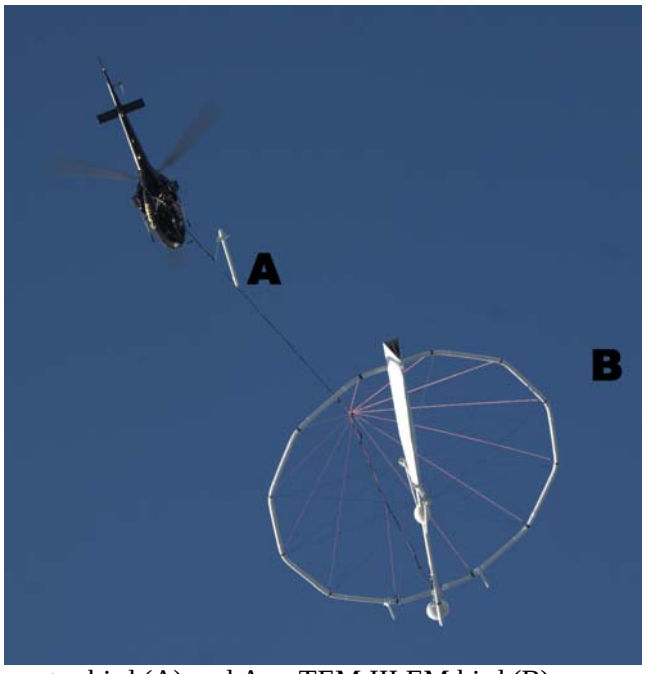

Figure 3. The magnetometer bird (A) and AeroTEM III EM bird (B)

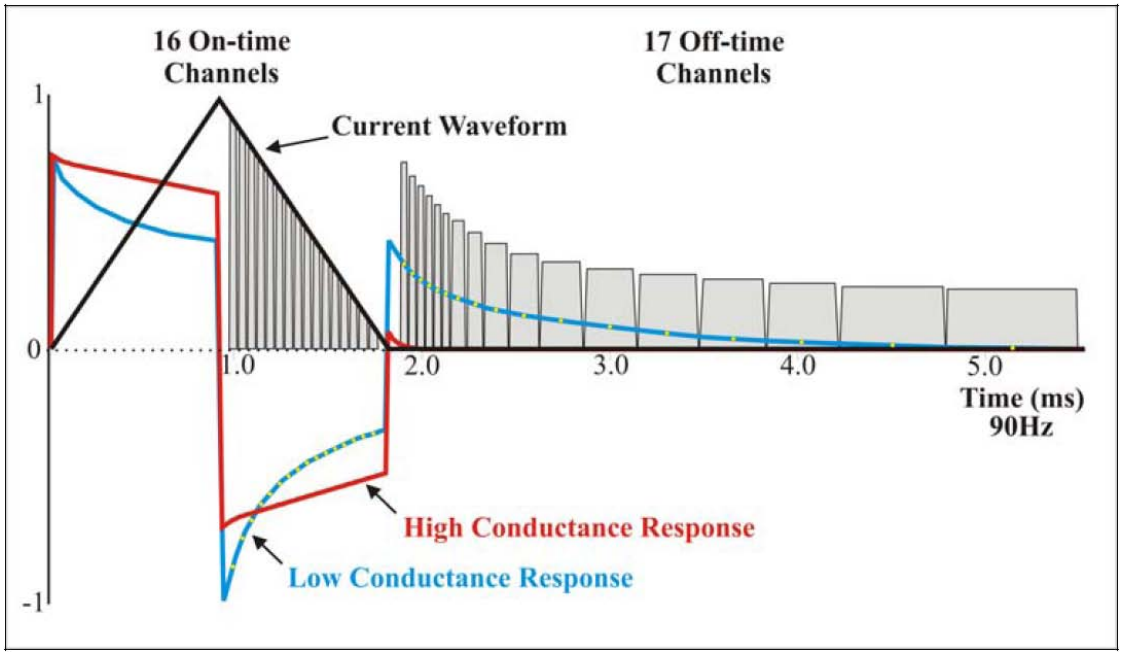

Figure 4. Schematic of Transmitter and Receiver waveforms

4.4. AERODAS ACQUISITION SYSTEM

The 200 channels of raw streaming data are recorded by the AeroDAS acquisition system (Figure 5) onto a removable hard drive. In addition the magnetic, altimeter and position data are also recorded in it, six channels of real time processed off-time EM decay in the Z direction and one in the X direction can be viewed on a color monitor on board, these channels are derived by a binning, stacking and filtering procedure on the raw streaming data.

The primary use of the displayed EM data (Z1 to Z6, X1), magnetic and altimeter is to provide for real-time QA/QC on board.

Figure 5. AeroTEM III Instrument Rack

The streaming data are processed post-survey to yield 33 stacked and binned on-time and off-time channels at a 10 Hz sample rate. The timing of the final processed EM channels is described in the following table:

Average TxOn -9.5288 us
Average TxSwitch 878.1358 us
Average TxOff 1702.5319 us

Channel	Sample Range	Time Width (us)	Time Center (us)	Time After TxOn (us)
On1	5 - 5	27.8	125.0	134.5
On2	6 - 6	27.8	152.8	162.3
On3	7 - 7	27.8	180.6	190.1
On4	8 - 8	27.8	208.3	217.9
On5	9 - 9	27.8	236.1	245.6
On6	10 - 10	27.8	263.9	273.4
On7	11 - 11	27.8	291.7	301.2
On8	12 - 12	27.8	319.4	329.0
On9	13 - 13	27.8	347.2	356.8
On10	14 - 14	27.8	375.0	384.5
On11	15 - 15	27.8	402.8	412.3
On12	16 - 16	27.8	430.6	440.1
On13	17 - 17	27.8	458.3	467.9
On14	18 - 18	27.8	486.1	495.6
On15	19 - 19	27.8	513.9	523.4
On16	20 - 20	27.8	541.7	551.2

Channel	Sample Range	Time Width (us)	Time Center (us)	Time After TxOff (us)
Off0	65 - 65	27.8	1791.7	89.1
Off1	66 - 66	27.8	1819.4	116.9
Off2	67 - 67	27.8	1847.2	144.7
Off3	68 - 68	27.8	1875.0	172.5
Off4	69 - 69	27.8	1902.8	200.2
Off5	70 - 70	27.8	1930.6	228.0
Off6	71 - 73	83.3	1986.1	283.6
Off7	74 - 76	83.3	2069.4	366.9
Off8	77 - 79	83.3	2152.8	450.2
Off9	80 - 82	83.3	2236.1	533.6
Off10	83 - 87	138.9	2347.2	644.7
Off11	88 - 92	138.9	2486.1	783.6
Off12	93 - 99	194.4	2652.8	950.2
Off13	100 - 109	277.8	2888.9	1186.4
Off14	110 - 124	416.7	3236.1	1533.6
Off15	125 - 148	666.7	3777.8	2075.2
Off16	149 - 186	1055.6	4638.9	2936.4

4.5. MAGNETOMETER BASE STATION

The base magnetometer was a Geometrics G-859 caesium vapour magnetometer system with integrated GPS. Data logging and UTC time synchronisation was carried out within the magnetometer, with the GPS providing the timing signal. The data logging was configured to measure at 1.0 second intervals. Digital recording resolution was 0.001 nT. The sensor was placed on a tripod in an area of low magnetic gradient and free of cultural noise sources. A continuously updated display of the base station values was available for viewing and regularly monitored to ensure acceptable data quality and diurnal variation.

4.6. RADAR ALTIMETER

A Terra TRA 3500/TRI-30 radar altimeter is used to record terrain clearance. The antenna was mounted on the outside of the helicopter beneath the cockpit. Therefore, the recorded data reflect the height of the helicopter above the ground. The Terra altimeter has an altitude accuracy of +/- 1.5 metres.

4.7. VIDEO TRACKING AND RECORDING SYSTEM

A high resolution digital colour 8 mm video camera is used to record the helicopter ground flight path along the survey lines. The video is digitally annotated with GPS position and time and can be used to verify ground positioning information and cultural causes of anomalous geophysical responses.

Figure 6. Digital video camera typical mounting location.

4.8. GPS NAVIGATION SYSTEM

The navigation system consists of an Ag-Nav Incorporated AG-NAV2 GPS navigation system comprising a PC-based acquisition system, navigation software, a deviation indicator in front of the aircraft pilot to direct the flight, a full screen display with controls in front of the operator, a Mid-Tech RX400p WAAS-enabled GPS receiver mounted on the instrument rack and an antenna mounted on the magnetometer bird. WAAS (Wide Area Augmentation System) consists of approximately 25 ground reference stations positioned across the United States that monitor GPS satellite data. Two master stations located on the east and west coasts collect data from the reference stations and create a GPS correction message. This correction accounts for GPS satellite orbit and clock drift plus signal delays caused by the atmosphere and ionosphere. The corrected differential message is then broadcast through one of two geostationary satellites, or satellites with a fixed position over the equator. The corrected position has a published accuracy of less than 3 metres.

Survey co-ordinates are set up prior to the survey and the information is fed into the airborne navigation system. The co-ordinate system employed in the survey design was WGS84 [World] using the UTM zone 10 N projection. The real-time differentially corrected GPS positional data was recorded by the AeroDAS system in geodetic coordinates (latitude and longitude using WGS84) at 0.2 s intervals.

4.9. DIGITAL ACQUISITION SYSTEM

The AeroTEM received waveform sampled during on and off-time at 200 channels per decay, 180 times per second, was logged by the proprietary AeroDAS data acquisition system. The streaming data was recorded on a removable hard-drive and was later backed-up onto DVD-ROM from the field-processing computer.

5. PERSONNEL

The following Aeroquest personnel were involved in the project:

- Operations Project Manager: Troy Will
- Field Data Processor: Thomas Wade
- Field Operator: Viktor Shevchenko
- Data Interpretation and Reporting: Chris Kahue, Liz Johnson

The survey pilot, Ted Slavin, was employed directly by the helicopter operator – HiWood Helicopters Ltd.

6. DELIVERABLES

6.1. HARDCOPY DELIVERABLES

The report includes a set of four 1:10,000 maps and the following four geophysical data products are delivered:

- TMI –Total Magnetic Intensity (TMI) with line contours and EM anomaly symbols.
- Z1-OFF– AeroTEM Z1 Off-time with line contours, and EM anomaly symbols.
- EM – AeroTEM off-time profiles Z3 – Z13, and EM anomaly symbols.
- DTM – Digital Terrain Model with line contours, and EM anomaly symbols.
- RES – Early Off-Time Resistivity with line contours, and EM anomaly symbols.

The coordinate/projection system for the maps is NAD83 – UTM Zone 10 N. For reference, the latitude and longitude in WGS84 are also noted on the maps.

All the maps show flight path trace, skeletal topography, and conductor picks represented by an anomaly symbol classified according to calculated off-time conductance. The anomaly symbol is accompanied by postings denoting the calculated off-time conductance, a thick or thin classification and an anomaly identifier label. The anomaly symbol legend and survey specifications are displayed on the left margin of the maps.

6.2. DIGITAL DELIVERABLES

6.2.1. Final Database of Survey Data (.GDB)

The geophysical profile data is archived digitally in a Geosoft GDB binary format database. A description of the contents of the individual channels in the database can be found in Appendix 2. A copy of this digital data is archived at the Aeroquest head office in Mississauga.

6.2.2. Geosoft Grid files (.GRD)

Levelled Grid products used to generate the geophysical map images. All grids have 10 m cell size.

- Total Magnetic Intensity (10-007_magu.grd)
- AeroTEM Z Offtime Channel 1 (10-007_zoff1.grd)
- Digital Terrain Model (10-007_dtm.grd)
- Early Time Resistivity EM Channel 1 (10-007_Resistivity_ZOff1.grd)

- Restivity Depth Slice 100 Meters (10-007_Resistivity_100m.grd)
- Restivity Depth Slice 150 Meters (10-007_Resistivity_150m.grd)

6.2.3. Digital Versions of Final Maps (.MAP, .PDF)

Map files in Geosoft .map and Adobe PDF format.

6.2.4. Google Earth Files (.kmz)

Flight navigation lines, EM Anomalies and geophysical grids in Google earth kmz format. Double click to view in Google Earth.

6.2.5. Free Viewing Software (.EXE)

- Geosoft Oasis Montaj Viewing Software
- Adobe Acrobat Reader
- Google Earth Viewer

6.2.6. Digital Copy of this Document (.PDF)

Adobe PDF format of this document.

7. DATA PROCESSING AND PRESENTATION

All in-field and post-field data processing was carried out using Aeroquest proprietary data processing software and Geosoft Oasis Montaj software. Maps were generated using 36-inch and 42-inch wide Hewlett Packard ink-jet plotters.

7.1. BASE MAP

The geophysical maps accompanying this report are based on positioning in the NAD83 datum. The survey geodetic GPS positions have been projected using the Universal Transverse Mercator projection in Zone 10 North. A summary of the map datum and projection specifications is given following:

- Ellipse: GRS 1980
- Ellipse major axis: 6378137m eccentricity: 0.081819191
- Datum: North American 1983 - Canada Mean
- Datum Shifts (x,y,z) : 0, 0, 0 metres
- Map Projection: Universal Transverse Mercator Zone 10 (Central Meridian 123ºW)
- Central Scale Factor: 0.9996
- False Easting, Northing: 500,000m, 0m

For reference, the latitude and longitude in WGS84 are also noted on the maps.

The background vector topography was sourced from Natural Resources Canada 1:50000 National Topographic Data Base data and the background shading were derived from NASA Shuttle Radar Topography Mission (SRTM) 90 metre resolution DEM data.

7.2. FLIGHT PATH & TERRAIN CLEARANCE

The position of the survey helicopter was directed by use of the Global Positioning System (GPS). Positions were updated five times per second (5 Hz) and expressed as WGS84 latitude and longitude calculated from the raw pseudo range derived from the C/A code signal. The instantaneous GPS flight path, after conversion to UTM co-ordinates, is drawn using linear interpolation between the x/y positions. The terrain clearance was maintained with reference to the radar altimeter. The raw Digital Terrain Model (DTM) was derived by taking the GPS survey elevation and subtracting the radar altimeter terrain clearance values. The calculated topography elevation values are relative and are not tied in to surveyed geodetic heights.

Each flight included at least two high elevation 'background' checks. These high elevation checks are to ensure that the gain of the system remained constant and within specifications.

7.3. ELECTROMAGNETIC DATA

The raw streaming data, sampled at a rate of 36,000 Hz (200 channels, 180 times per second) was reprocessed using a proprietary software algorithm developed and owned by Aeroquest Limited. Processing involves the compensation of the X and Z component data for the primary field waveform. Coefficients for this compensation for the system transient are determined and applied to the stream data. The stream data are then pre-filtered, stacked, binned to the 33 on and off-time channels and checked for the effectiveness of the compensation and stacking processes. The stacked data is then filtered, levelled and split up into the individual line segments. Further base level adjustments may be carried out at this stage. The filtering of the stacked data is designed to remove or minimize high frequency noise that cannot be sourced from the geology.

The final field processing step was to merge the processed EM data with the other data sets into a Geosoft GDB file. The TS "time stamp" and EM Fiducial are used to synchronize the two datasets. The processed channels are merged into 'array format; channels in the final Geosoft database as Zon, Zoff, Xon, and Xoff.

Apparent bedrock EM anomalies were interpreted with the aid of an auto-pick from positive peaks and troughs in the off-time Z channel responses correlated with X channel responses. The auto-picked anomalies were reviewed and edited by a geophysicist on a line by line basis to discriminate between thin and thick conductor types. Anomaly picks locations were migrated and removed as required. This process ensures the optimal representation of the conductor centres on the maps.

At each conductor pick, estimates of the off-time conductance have been generated based on a horizontal plate source model for those data points along the line where the response amplitude is sufficient to yield an acceptable estimate. Some of the EM anomaly picks do not display a Tau value; this is due to the inability to properly define the decay of the conductor usually because of low signal amplitudes. Each conductor pick was then classified according to a set of seven ranges of calculated off-time conductance values. For high conductance sources, the on-time conductance values may be used, since it provides a more accurate measure of high-conductance sources. Each symbol is also given an identification letter label, unique to each flight line. Conductor picks that did not yield an acceptable estimate of off-time conductance due to a low amplitude response were classified as a low conductance source. Please refer to the anomaly symbol legend located in the margin of the maps.

7.4. MAGNETIC DATA

Prior to any levelling the magnetic data was subjected to a lag correction of -0.1 seconds and a spike removal filter. The filtered aeromagnetic data were then corrected for diurnal variations using the magnetic base station and the intersections of the tie lines. No corrections for the regional reference field (IGRF) were applied. The corrected profile data were interpolated on to a grid using a bi-directional grid technique with a grid cell size of 10 metres. The final levelled grid provided the basis for threading the presented contours which have a minimum contour interval of 5 nT.

8. GENERAL COMMENTS

The survey was successful in mapping the magnetic and conductive properties of the geology throughout the survey area. Below is a brief interpretation of the results. For a detailed interpretation please contact Aeroquest Limited.

8.1. MAGNETIC RESPONSE

The magnetic data provide a high resolution map of the distribution of the magnetic mineral content of the survey area. This data can be used to interpret the location of geological contacts and other structural features such as faults and zones of magnetic alteration. The sources for anomalous magnetic responses are generally thought to be predominantly magnetite because of the relative abundance and strength of response (high magnetic susceptibility) of magnetite over other magnetic minerals such as pyrrhotite.

8.2. APPARENT RESISTIVITY

Apparent resistivity was computed from the off-time z-component data at each measurement location. The algorithm uses the pseudo-layer half-space model (Huang, H. and Rudd, J., 2008). The primary advantages of this method are immunity to altimeter errors, and better resolution of conductive layers than other methods. A table lookup procedure is established based on the analytic solution of a half-space model to speed up the processing. This method can be expanded to generate depth section images (CDIs). The effective depths for the sections are derived empirically from the computed diffusion depth and apparent thickness of the pseudo-layer.

The computed resistivity values were interpolated onto a 10 m regular grid, using the bi-gridding algorithm, and then clipped with minimum and maximum values of 0 and 995 and finally applied hanning filter.

8.3. EM ANOMALIES

The EM anomalies on the maps are classified by conductance (as described earlier in the report) and also by the thickness of the source. A thin, vertically orientated source produces a double peak anomaly in the z-component response and a positive to negative crossover in the x-component response (Figure 7). For a vertically orientated thick source (say, greater than 10 metres), the response is a single peak in the z-component response and a negative to positive crossover in the x-component response (Figure 8). Because of these differing responses, the AeroTEM system provides discrimination of thin and thick sources and this distinction is indicated on the EM anomaly symbols (N = thin and K = thick). Where multiple, closely spaced conductive sources occur, or where the source has a shallow dip, it can be difficult to uniquely determine the type (thick vs. thin) of the source (Figure 9). In

these cases both possible source types may be indicated by picking both thick and thin response styles. For shallow dipping conductors the 'thin' pick will be located over the edge of the source, whereas the 'thick' pick will fall over the downdip 'heart' of the anomaly.

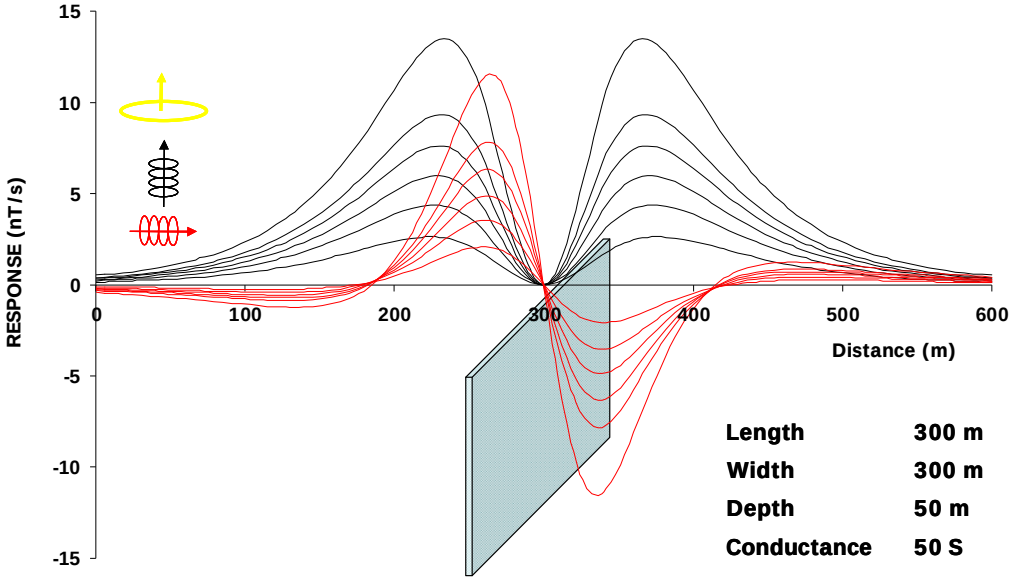

Figure 7. AeroTEM response to a 'thin' vertical conductor.

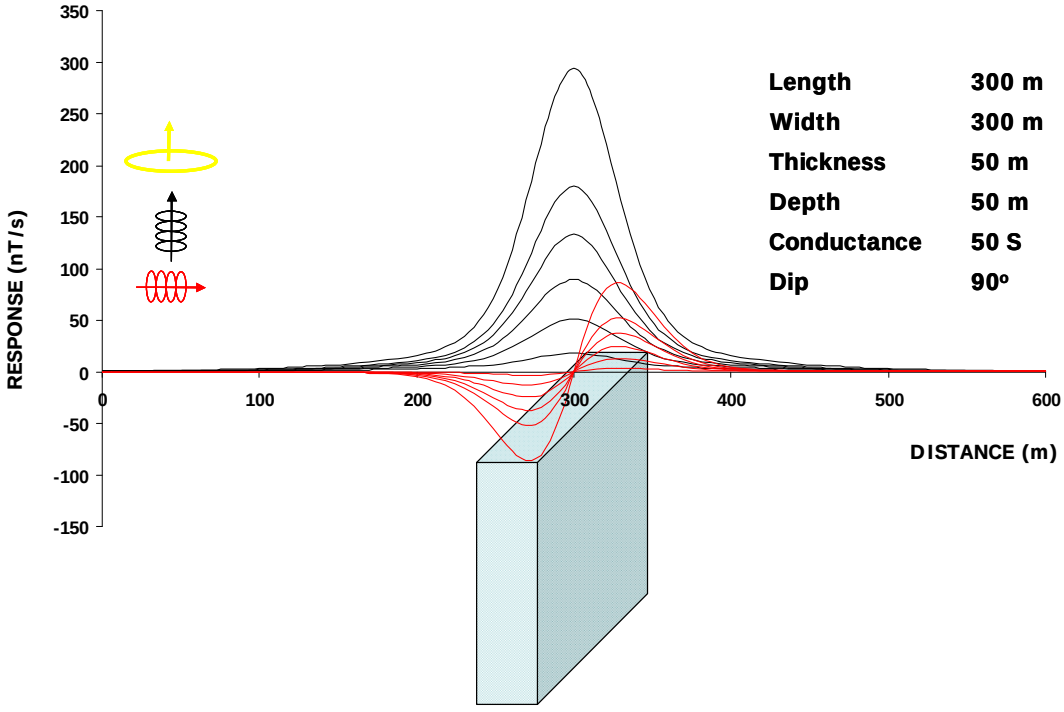

Figure 8. AeroTEM response for a 'thick' vertical conductor.

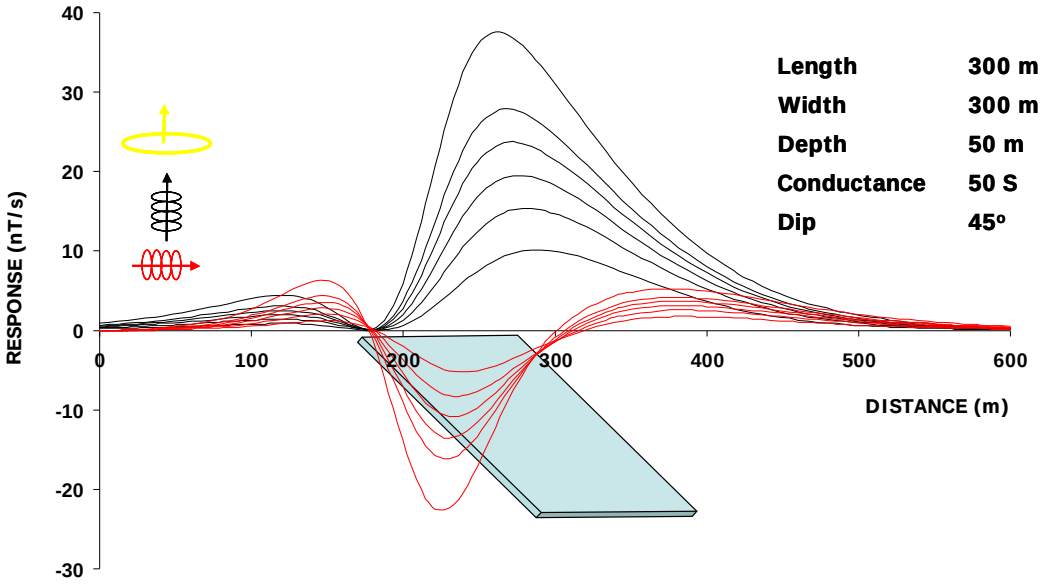

Figure 9. AeroTEM response over a 'thin' dipping conductor.

All cases should be considered when analyzing the interpreted picks and prioritizing for follow-up. Specific anomalous responses which remain as high priority should be subjected to numerical modeling prior to drill testing to determine the dip, depth and probable geometry of the source.

APPENDIX 1: SURVEY BOUNDARIES

The following table presents the block boundaries. All geophysical data presented in this report have been windowed to 100m outside of these boundaries. X and Y positions are in metres: NAD83 UTM Zone 10 N.

Rabbit Mine Property:

X	Y
654376.0	5494794.0
657274.0	5495566.0
657274.0	5495566.0
657296.0	5495520.0
658648.0	5495160.0
659860.0	5495160.0
659860.0	5492431.0
659902.0	5492390.0
661254.0	5492031.0
661251.0	5492001.0
658355.0	5491218.0
658357.0	5491249.0
657005.0	5491614.0
656852.0	5491625.0
655750.0	5491625.0
655749.0	5494383.0
654397.0	5494748.0
654376.0	5494792.0

APPENDIX 2: DESCRIPTION OF DATABASE FIELDS

The GDB file is a Geosoft binary database. In the database, the Survey lines and Tie Lines are prefixed with an "L" for "Line" and "T" for "Tie".

COLUMN	UNITS	DESCRIPTOR
line	#	Line number
flight	#	Flight #
emfid	#	AERODAS Fiducial
utctime	hh:mm:ss.ss	UTC time
x	M	UTM Easting (NAD83, Zone 10)
y	M	UTM Northing (NAD83, Zone 10)
galt	M	GPS elevation of magnetometer bird
ralt	M	Helicopter radar altimeter (height above terrain)
bheight	M	Terrain clearance of EM bird
basemag	nT	Base station total magnetic intensity
magU	nT	Final levelled total magnetic intensity from upper magnetometer sensor (installed on the tail of the EM bird).
dtm	M	Digital Terrain Model
zon	nT/s	EM On-Time Z component Channels 1-16
zoff	nT/s	EM Off-Time Z component Channels 0-16
Xon	nT/s	EM On-Time X component Channels 1-16
Xoff	nT/s	EM Off-Time X component Channels 0-16
pwrline	#	powerline monitor data channel
Grade	#	Classification from 1-7 based on conductance of conductor pick
Anom_Labels		Letter label of conductor pick (Unique per flight line)
Off_Con	S	Off-time conductance at conductor pick
Off_Tau	µs	Off-time decay constant at conductor pick
Anom_ID	K/N	EM Anomaly response style (K= thicK, N = thiN)
Off_AllCon	S	Off-time conductance
Off_AllTau	µs	Off-time decay constant
TranOff	S	Transmitter turn off time
TranOn	S	Transmitter turn on time
TranPeak	A	Transmitter peak current
TranSwitch	S	Transmitter peak current time
Off_Pick	#	Anomaly pick channel
Res100m	Ωm	Resistivity at 100 m depth
Res150m	Ωm	Resistivity at 150 m depth
ResOff1	Ωm	Early time Resistivity

APPENDIX 3: AEROTEM ANOMALY LISTING

Rabbitt Mine:

Line	Anom	ID	Cond (S)	Tau (µs)	Flight #	UTC Time	Bird height (m)	Easting (m)	Northing (m)
10011	A	K	1.5	124.1	5	20:56:08	41.5	657151.0	5495539.3
10021	A	K	1.2	107.3	5	20:58:06	56.2	657167.7	5495458.2
10031	A	K	1.0	97.5	5	21:03:09	43.6	657179.4	5495438.7
10041	A	K	0.9	92.7	5	21:04:47	51.6	657181.8	5495388.3
10051	A	K	1.4	119.5	5	21:12:00	48.4	657194.6	5495333.3
10061	A	K	1.1	103.3	5	21:13:41	58.6	657196.5	5495282.1
10071	A	K	1.7	128.8	5	21:18:13	59.7	657207.9	5495233.6
10081	A	K	1.1	103.8	5	21:20:23	53.7	657209.7	5495188.4
10091	A	K	1.2	110.6	5	21:24:38	44.6	657215.5	5495137.9
10101	A	K	1.2	108.2	5	21:27:05	53.1	657220.0	5495092.4
10111	A	K	1.4	116.0	5	21:31:08	49.2	657222.4	5495024.4
10121	A	K	1.3	111.6	5	21:33:28	49.2	657223.6	5494980.4
10131	A	K	1.4	117.9	5	21:37:04	43.5	657215.5	5494936.1
10140	A	K	1.7	129.4	2	18:51:27	56.1	657208.6	5494880.2
10150	A	K	2.5	159.3	2	18:54:55	66.8	657193.7	5494825.7
10160	A	K	2.2	148.5	2	18:58:03	61.6	657175.7	5494760.7
10170	A	K	2.3	150.8	2	19:01:11	68.4	657171.6	5494709.9
10180	A	K	4.7	216.8	2	19:04:25	67.4	657174.3	5494653.3
10190	A	K	11.1	332.9	2	19:10:03	91.7	657181.4	5494606.5
10200	A	K	8.2	286.3	2	19:13:41	83.7	657188.0	5494560.1
10210	A	K	2.8	166.2	2	19:16:48	79.0	657206.8	5494507.2
10220	A	K	3.6	190.4	2	19:21:04	78.5	657216.9	5494469.2
10230	A	K	4.5	212.7	2	19:24:06	65.4	657225.9	5494420.1
10240	A	K	8.8	295.9	2	19:28:27	64.2	657238.0	5494371.4
10250	A	K	9.8	312.3	2	19:31:36	73.3	657273.1	5494322.1
10260	A	K	8.4	290.1	2	19:35:51	69.8	657326.7	5494292.0
10260	B	K	49.7	704.6	2	19:36:15	62.5	656702.0	5494124.7
10270	A	K	2.2	148.5	2	19:39:02	78.7	657365.2	5494234.6
10280	A	K	5.2	226.9	2	19:46:34	67.1	657403.4	5494209.2
10290	A	K	2.5	158.3	2	19:49:51	70.6	657429.3	5494156.4
10300	A	K	2.4	155.7	2	19:54:11	58.4	657452.2	5494115.9
10310	A	K	1.1	106.6	2	19:57:26	67.5	657475.0	5494070.4
10320	A	K	2.1	145.7	2	20:01:44	64.0	657493.1	5494023.7
10330	A	K	1.8	133.2	2	20:05:00	67.6	657516.6	5493969.5
10340	A	K	2.2	147.8	2	20:09:06	79.3	657532.1	5493928.0
10350	A	K	1.6	125.8	2	20:12:12	74.3	657559.3	5493876.6
10360	A	K	1.5	122.7	2	20:16:31	75.7	657595.0	5493836.5
10370	A	K	1.9	137.2	2	20:19:54	67.1	657637.6	5493801.3
10380	A	K	0.8	86.4	3	21:50:13	68.5	657656.5	5493764.6
10380	B	K	0.6	75.5	3	21:51:26	60.2	655691.1	5493228.8
10390	A	K	1.0	98.6	3	21:52:28	66.2	655706.6	5493172.3

Line	Anom	ID	Cond (S)	Tau (µs)	Flight #	UTC Time	Bird height (m)	Easting (m)	Northing (m)
10390	B	K	0.8	86.4	3	21:54:00	69.6	657684.1	5493712.8
10400	A	K	2.1	144.4	3	21:58:29	68.2	657705.4	5493670.7
10400	B	K	1.4	118.9	3	21:59:39	62.3	655730.8	5493134.1
10410	A	K	2.3	150.9	3	22:00:38	77.5	655753.3	5493096.1
10410	B	K	0.9	93.3	3	22:02:05	69.5	657737.9	5493625.8
10420	A	K	5.4	232.1	3	22:06:08	66.5	657777.5	5493579.5
10420	B	K	2.1	144.8	3	22:07:22	66.3	655760.3	5493041.4
10430	A	K	2.7	164.8	3	22:08:25	73.7	655781.3	5492999.5
10430	B	K	1.1	102.9	3	22:09:50	66.4	657811.2	5493538.6
10440	A	K	5.5	234.4	3	22:13:38	59.2	657851.4	5493493.8
10440	B	K	0.9	97.0	3	22:14:51	67.6	655795.6	5492948.6
10450	A	K	2.9	171.2	3	22:15:58	69.5	655808.0	5492890.9
10450	B	K	0.8	88.5	3	22:17:29	67.5	657888.1	5493462.9
10460	A	K	2.5	157.4	3	22:21:00	55.2	657914.3	5493409.8
10460	B	K	0.9	95.9	3	22:22:17	73.3	655809.1	5492843.6
10470	A	K	2.0	140.9	3	22:23:23	80.4	655842.1	5492792.5
10470	B	K	1.1	106.4	3	22:24:46	60.3	657928.5	5493369.4
10480	A	K	1.4	116.6	3	22:28:04	55.8	657929.3	5493310.0
10480	B	K	1.2	107.3	3	22:29:18	73.6	655876.0	5492757.2
10500	A	K	0.5	72.4	3	22:40:03	64.0	656254.6	5492753.4
10510	A	K	0.9	93.5	3	22:41:47	68.8	656274.0	5492705.7
10520	A	K	0.7	83.7	3	22:47:19	67.2	656291.6	5492665.2
10530	A	K	1.5	120.7	3	22:49:03	54.6	656273.2	5492602.5
10540	A	K	0.9	92.6	3	22:54:24	65.0	656278.5	5492548.3
10550	A	K	1.7	128.5	3	22:56:06	62.6	656264.9	5492493.3
10550	B	K	5.3	229.2	3	22:58:34	55.1	659788.8	5493443.5
10560	A	K	3.5	187.6	3	22:59:33	65.1	659776.5	5493388.3
10560	B	K	0.7	82.9	3	23:01:45	68.7	656237.6	5492440.4
10570	A	K	2.1	146.2	3	23:03:13	72.1	656230.7	5492383.1
10570	B	K	2.9	169.7	3	23:05:49	62.8	659884.9	5493371.8
10580	A	K	2.4	153.6	3	23:06:42	74.5	659813.7	5493302.2
10580	B	K	0.4	60.5	3	23:08:54	68.6	656227.8	5492329.3
10590	A	K	0.8	88.8	3	23:10:18	78.7	656202.2	5492291.4
10590	B	K	3.6	190.6	3	23:12:56	66.3	659883.1	5493265.5
10600	A	K	3.5	186.6	3	23:13:45	79.3	659899.6	5493207.2
10600	B	K	0.7	82.4	3	23:16:15	77.2	656161.9	5492210.3
10610	A	K	1.0	97.4	3	23:17:39	79.3	656161.5	5492165.7
10610	B	K	4.5	212.3	3	23:20:20	55.3	659888.6	5493154.2
10620	A	K	7.2	268.0	4	17:18:05	48.9	659874.1	5493099.5
10620	B	K	0.8	87.2	4	17:21:38	79.0	656140.2	5492099.1
10630	A	K	1.2	107.5	4	17:23:59	59.9	656166.7	5492072.9
10630	B	K	4.7	217.5	4	17:27:15	53.3	659690.9	5493003.1
10640	A	K	4.6	214.9	4	17:28:24	64.1	659745.5	5492981.2
10640	B	K	0.7	84.3	4	17:31:46	50.6	656172.8	5492016.2
10650	A	K	1.1	104.1	4	17:33:32	61.5	656168.3	5491963.0

Line	Anom	ID	Cond (S)	Tau (µs)	Flight #	UTC Time	Bird height (m)	Easting (m)	Northing (m)
10650	B	K	6.0	243.9	4	17:36:42	46.1	659815.0	5492942.3
10660	A	K	9.7	311.0	4	17:37:38	49.1	659890.5	5492901.2
10660	B	K	0.6	78.1	4	17:41:01	88.2	656207.7	5491917.7
10670	A	K	0.8	87.0	4	17:43:01	44.1	656232.6	5491862.0
10680	A	K	0.6	79.1	4	17:49:56	64.8	656227.6	5491812.6
10690	A	K	0.7	82.5	4	17:51:40	41.2	656246.8	5491766.9
10700	A	K	0.9	92.8	4	18:03:10	48.8	656247.3	5491728.7
10710	A	K	0.3	53.1	4	18:04:39	49.0	656222.8	5491662.6
10720	A	K	12.6	355.4	4	18:08:21	43.7	659784.2	5492567.9
10720	B	K	0.6	80.0	4	18:11:38	52.5	656218.2	5491627.0
10720	A	K	0.4	61.6	4	18:12:39	64.4	656312.2	5491593.6
10720	B	K	12.7	356.9	4	18:15:38	64.7	659844.6	5492538.1
10740	A	K	16.6	407.3	4	18:16:35	60.6	659934.8	5492508.9
10750	A	K	5.9	243.1	4	18:22:38	54.4	659748.4	5492401.4
10760	A	K	6.5	255.7	4	18:23:39	58.3	659705.6	5492345.0
10770	A	K	9.7	311.6	4	18:29:06	49.8	659742.8	5492286.2
10790	A	K	13.9	372.6	4	18:35:37	69.8	659792.8	5492202.3
10790	B	K	19.3	439.5	4	18:36:03	68.7	660324.8	5492342.4
10800	A	K	15.6	395.4	4	18:37:05	61.8	659805.5	5492156.7
10800	B	K	1.1	106.3	4	18:38:25	54.8	658088.2	5491707.1
10810	A	K	0.9	92.1	4	18:40:14	52.8	658117.0	5491644.1
10810	B	K	13.5	367.1	4	18:41:38	57.7	659832.0	5492114.7
10810	C	K	22.0	468.9	4	18:42:02	61.6	660330.3	5492252.8
10820	A	K	22.5	474.1	5	20:18:45	66.7	660251.2	5492170.7
10820	B	K	2.5	158.3	5	20:20:38	58.1	658135.7	5491609.9
10830	A	K	1.1	103.6	5	20:22:15	48.9	658190.5	5491560.6
10830	B	K	23.8	487.6	5	20:23:56	58.1	660260.0	5492116.1
10840	A	K	21.0	458.0	5	20:25:50	65.7	660265.5	5492064.9
10840	B	K	1.7	131.5	5	20:27:18	56.2	658306.2	5491547.0
10850	A	K	3.8	195.8	5	20:28:53	58.3	658350.3	5491499.5
10850	B	K	35.0	592.0	5	20:30:13	49.9	660270.3	5492015.2
10860	A	K	40.9	639.2	5	20:32:20	54.0	660271.3	5491977.5
10860	B	K	1.1	106.1	5	20:33:33	47.3	658423.7	5491477.7
10870	A	K	0.7	83.5	5	20:35:14	47.6	658470.8	5491429.7
10870	B	K	35.5	595.9	5	20:36:28	46.4	660255.8	5491911.8
10880	A	K	34.7	589.3	5	20:39:09	55.2	660246.7	5491860.7
10880	B	K	0.6	79.2	5	20:40:19	47.5	658550.4	5491404.5
10890	A	K	0.5	71.4	5	20:41:50	50.4	658587.7	5491354.3
10890	B	K	35.6	596.2	5	20:42:58	39.0	660190.2	5491792.3
10900	A	K	36.9	607.4	5	20:46:27	64.3	660050.8	5491698.5
10900	B	K	0.6	79.4	5	20:47:24	59.8	658596.7	5491324.1
19040	A	K	1.0	100.4	1	20:37:42	60.4	656544.7	5494123.7
19050	A	K	11.8	342.8	1	20:32:36	79.6	657025.4	5494236.8
19060	A	K	8.8	297.2	1	20:27:31	54.4	658271.8	5491534.6
19060	B	K	2.6	161.6	1	20:29:29	75.0	657636.5	5493900.2

Line	Anom	ID	Cond (S)	Tau (µs)	Flight #	UTC Time	Bird height (m)	Easting (m)	Northing (m)
19060	C	K	4.1	202.1	1	20:30:36	57.9	657244.1	5495375.5
19070	A	K	2.0	140.8	1	20:26:06	80.4	658828.6	5491353.0
19100	A	K	46.8	683.9	1	20:09:28	58.3	660255.3	5491890.5

APPENDIX 4: AEROTEM DESIGN CONSIDERATIONS

Helicopter-borne EM systems offer an advantage that cannot be matched from a fixed-wing platform. The ability to fly at slower speed and collect dat

3a with high spatial resolution, and with great accuracy, means the helicopter EM systems provide more detail than any other EM configuration, airborne or ground-based. Spatial resolution is especially important in areas of complex geology and in the search for discrete conductors. With the advent of helicopter-borne high-moment time domain EM systems the fixed wing platforms are losing their *only* advantage – depth penetration.

Advantage 1 – Spatial Resolution

The AeroTEM system is specifically designed to have a small footprint. This is accomplished through the use of concentric transmitter-receiver coils and a relatively small diameter transmitter coil (5 m). The result is a highly focused exploration footprint, which allows for more accurate "mapping" of discrete conductors. Consider the transmitter primary field images shown in Figure 1, for AeroTEM versus a fixed-wing transmitter.

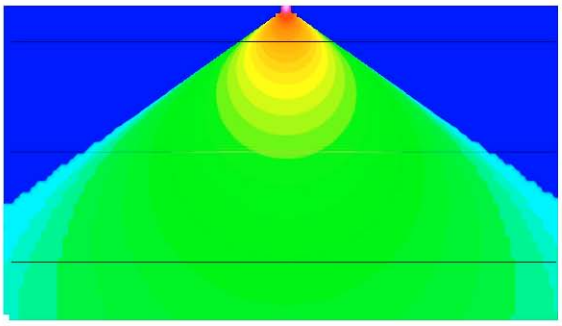

The footprint of AeroTEM at the earth's surface is roughly 50m on either side of transmitter

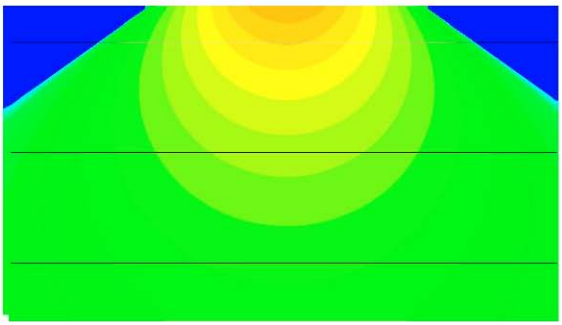

The footprint of a fixed-wing system is roughly 150 m on either side of the transmitter

Figure 1. A comparison of the footprint between AeroTEM and a fixed-wing system, highlights the greater resolution that is achievable with a transmitter located closer to the earth's surface. The AeroTEM footprint is one third that of a fixed-wing system and is symmetric, while the fixed-wing system has even lower spatial resolution along the flight line because of the separated transmitter and receiver configuration.

At first glance one may want to believe that a transmitter footprint that is distributed more evenly over a larger area is of benefit in mineral exploration. In fact, the opposite is true; by energizing a larger surface area, the ability to energize and detect discrete conductors is reduced. Consider, for example, a comparison between AeroTEM and a fixed-wing system over the Mesamax Deposit (1,450,000 tonnes of 2.1% Ni, 2.7% Cu, 5.2 g/t Pt/Pd). In a test survey over three flight lines spaced 100 m apart, AeroTEM detected the Deposit on all three flight lines. The fixed-wing system detected the Deposit only on two flight lines. In exploration programs that seek to expand the flight line spacing in an effort to reduce the cost of the airborne survey, discrete conductors such as the Mesamax Deposit can go undetected. The argument often put forward in favour of using fixed-wing systems is that because of their larger footprint, the flight line spacing can indeed be widened. Many fixed-wing surveys are flown at 200 m or 400 m. Much of the survey work performed by Aeroquest has been to survey in areas that were previously flown at these wider line spacings. One of the reasons for AeroTEM's impressive discovery record has been the strategy of flying closely spaced lines and finding all the discrete near-surface conductors. These higher resolution surveys are being flown within existing mining camps, areas that improve the chances of discovery.

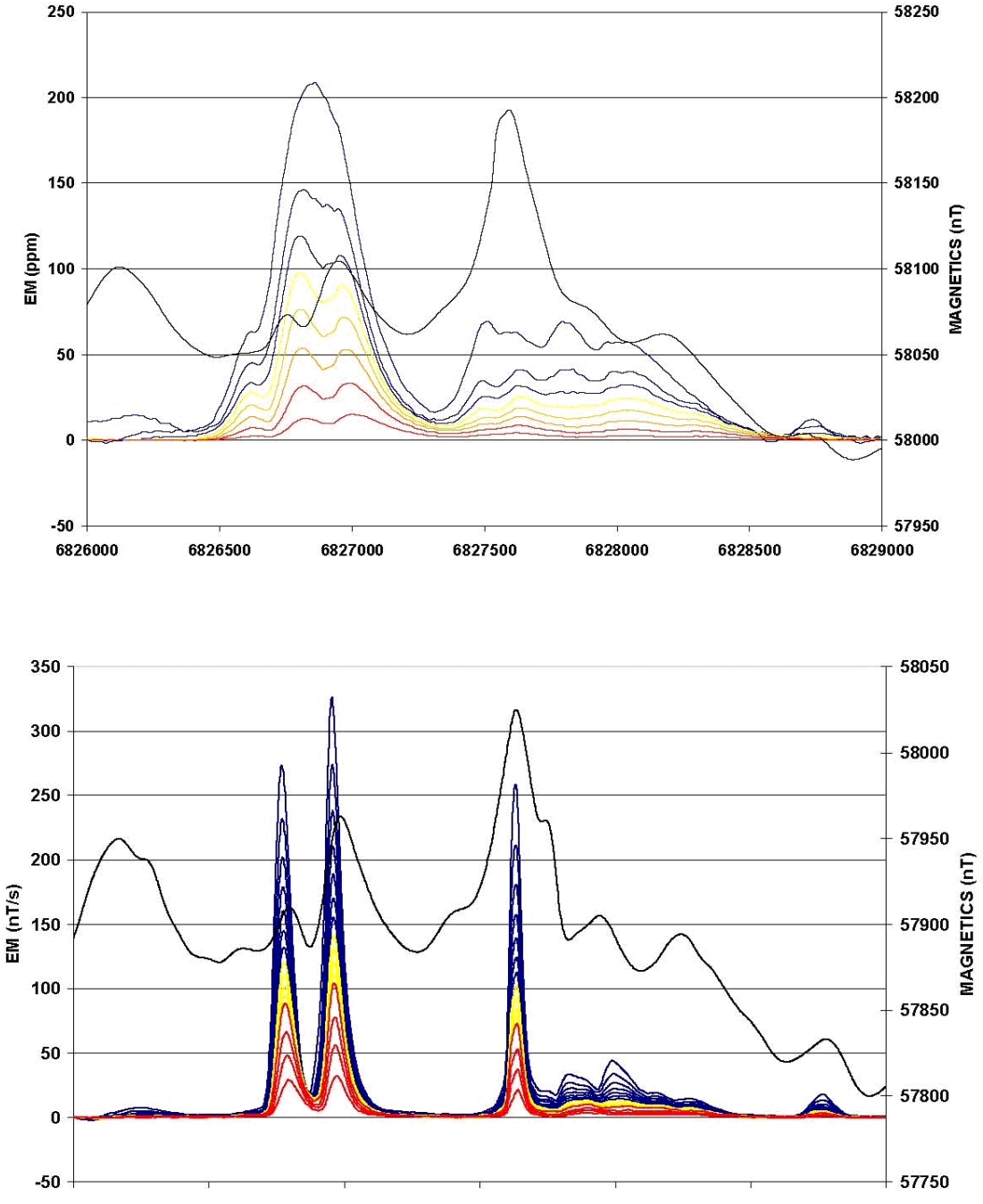

Figure 2. Fixed-wing (upper) and AeroTEM (lower) comparison over the eastern limit of the Mesamax Deposit, a Ni-Cu-PGE zone located in the Raglan nickel belt and owned by Canadian Royalties. Both systems detected the Deposit further to the west where it is closer to surface.

The small footprint of AeroTEM combined with the high signal to noise ratio (S/N) makes the system more suitable to surveying in areas where local infrastructure produces electromagnetic noise, such as power lines and railways. In 2002 Aeroquest flew four exploration properties in the Sudbury Basin that were under option by FNX Mining Company Inc. from Inco Limited. One such property, the Victoria Property, contained three major power line corridors.

The resulting AeroTEM survey identified all the known zones of Ni-Cu-PGE mineralization, and detected a response between two of the major power line corridors but in an area of favourable geology. Three boreholes were drilled to test the anomaly, and all three intersected sulphide. The third borehole encountered 1.3% Ni, 6.7% Cu, and 13.3 g/t TPMs over 42.3 ft. The mineralization was subsequently named the Powerline Deposit.

The success of AeroTEM in Sudbury highlights the advantage of having a system with a small footprint, but also one with a high S/N. This latter advantage is achieved through a combination of a high-moment (high signal) transmitter and a rigid geometry (low noise). Figure 3 shows the Powerline Deposit response and the response from the power line corridor at full scale. The width of power line response is less than 75 m.

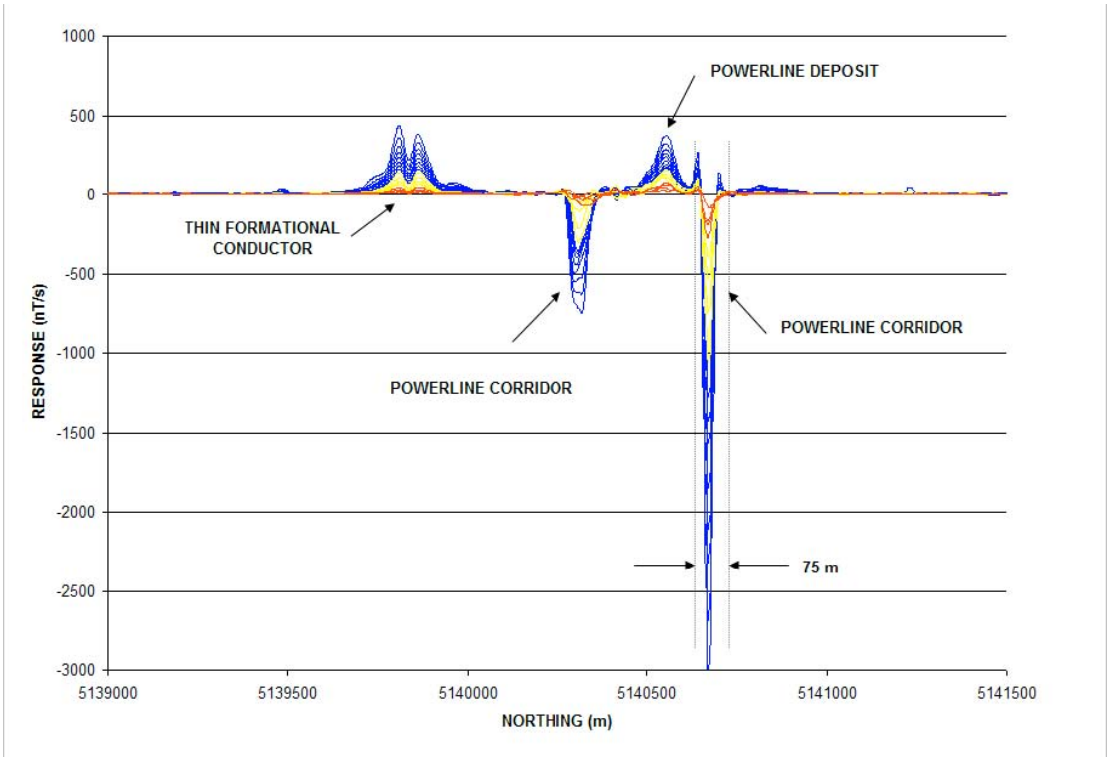

Figure 3. The Powerline Deposit is located between two major power line corridors, which make EM surveying problematic. Despite the strong response from the power line, the anomaly from the Deposit is clearly detected. Note the thin formational conductor located to the south. The only way to distinguish this response from that of two closely spaced conductors is by interpreting the X-axis coil response.

Advantage 2 – Conductance Discrimination

The AeroTEM system features full waveform recording and as such is able to measure the on-time response due to high conductance targets. Due to the processing method (primary field removal), there is attenuation of the response with increasing conductance, but the AeroTEM on-time measurement is still superior to systems that rely on lower base frequencies to detect high conductance targets, but do not measure in the on-time.

The peak response of a conductive target to an EM system is a function of the target conductance and the EM system base frequency. For time domain EM systems that measure only in the off-time, there is a drop in the peak response of a target as the base frequency is lowered for all conductance values below the peak system response. For example, the AeroTEM peak response occurs for a 10 S conductor in the early off-time and 100 S in the late off-time for a 150 Hz base frequency. Because base frequency and conductance form a linear relationship when considering the peak response of any EM system, a drop in base frequency of 50% will double the conductance at which an EM system shows its peak response. If the base frequency were lowered from 150 Hz to 30 Hz there would be a fivefold increase in conductance at which the peak response of an EM occurred.

However, in the search for highly conductive targets, such as pyrrhotite-related Ni-Cu-PGM deposits, a fivefold increase in conductance range is a high price to pay because the signal level to lower conductance targets is reduced by the same factor of five. For this reason, EM systems that operate with low base frequencies are not suitable for general exploration unless the target conductance is more than 100 S, or the target is covered by conductive overburden.

Despite the excellent progress that has been made in modeling software over the past two decades, there has been little work done on determining the optimum form of an EM system for mineral exploration. For example, the optimum configuration in terms of geometry, base frequency and so remain unknown. Many geophysicists would argue that there is no single ideal configuration, and that each system has its advantages and disadvantages. We disagree.

When it comes to detecting and discriminating high-conductance targets, it is necessary to measure the pure in phase response of the target conductor. This measurement requires that the measured primary field from the transmitter be subtracted from the total measured response such that the secondary field from the target conductor can be determined. Because this secondary field is in-phase with the transmitter primary field, it must be made while the transmitter is turned on and the transmitter current is changing. The transmitted primary field is several orders of magnitude larger than the secondary field. AeroTEM uses a bucking coil to reduce the primary field at the receiver coils. The only practical way of removing the primary field is to maintain a rigid geometry between the transmitter, bucking and receiver coils. This is the main design consideration of the AeroTEM airframe and it is the only time domain airborne system to have this configuration.

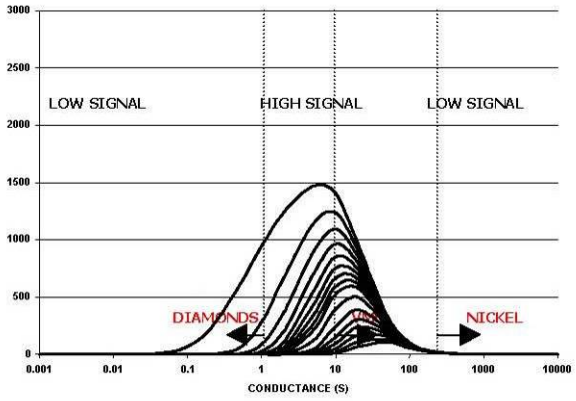

The off-time AeroTEM response for the 16 channel configuration.

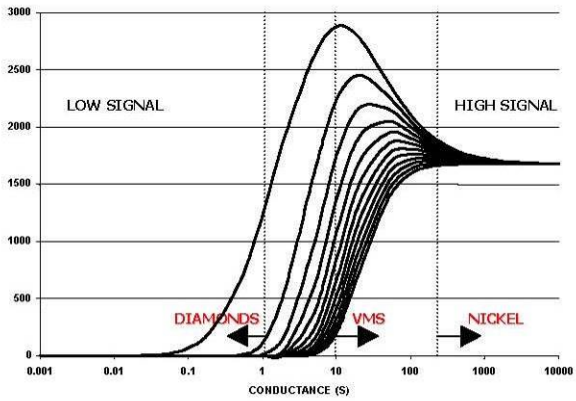

The on-time response assuming 100% removal of the measured primary field.

Figure 4. The off-time and on-time response nomogram of AeroTEM for a base frequency of 150 Hz. The on-time response is much stronger for higher conductance targets and this is why on-time measurements are more important than lower frequencies when considering high conductance targets in a resistive environment.

Advantage 3 – Multiple Receiver Coils

AeroTEM employs two receiver coil orientations. The Z-axis coil is oriented parallel to the transmitter coil and both are horizontal to the ground. This is known as a maximum coupled configuration and is optimal for detection. The X-axis coil is oriented at right angles to the transmitter coil and is oriented along the line-of-flight. This is known as a minimum coupled configuration, and provides information on conductor orientation and thickness. These two coil configurations combined provide important information on the position, orientation, depth, and thickness of a conductor that cannot be matched by the traditional geometries of the HEM or fixed-wing systems. The responses are free from a system geometric effect and can be easily compared to model type curves in most cases. In other words, AeroTEM data is very easy to interpret. Consider, for example, the following modeled profile:

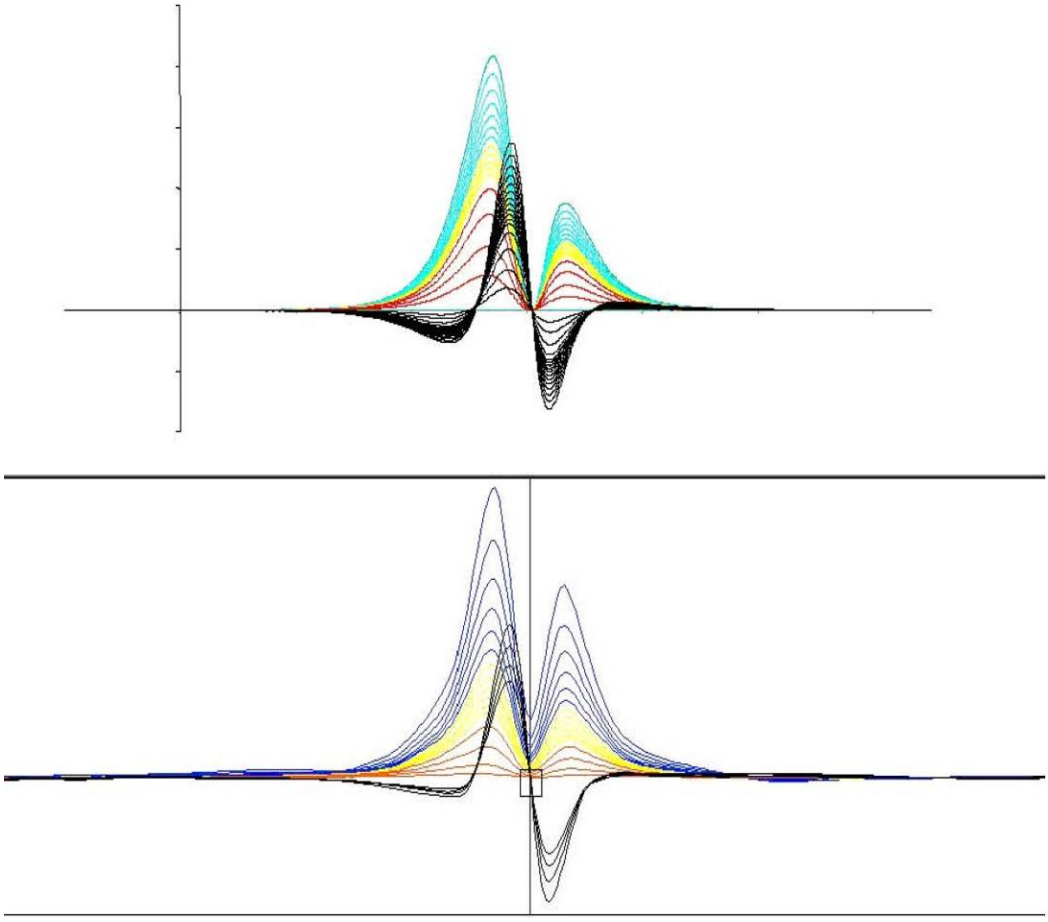

Figure 5. Measured (lower) and modeled (upper) AeroTEM responses are compared for a thin steeply dipping conductor. The response is characterized by two peaks in the Z-axis coil, and a cross-over in the X-axis coil that is centered between the two Z-axis peaks. The conductor dips toward the higher amplitude Z-axis peak. Using the X-axis cross-over is the only way of differentiating the Z-axis response from being two closely spaced conductors.

HEM versus AeroTEM

Traditional helicopter EM systems operate in the frequency domain and benefit from the fact that they use narrowband as opposed to wide-band transmitters. Thus all of the energy from the transmitter is concentrated in a few discrete frequencies. This allows the systems to achieve excellent depth penetration (up to 100 m) from a transmitter of modest power. The Aeroquest Impulse system is one implementation of this technology.

The AeroTEM system uses a wide-band transmitter and delivers more power over a wide frequency range. This frequency range is then captured into 16 time channels, the early channels containing the high frequency information and the late time channels containing the low frequency information down to the system base frequency. Because frequency domain HEM systems employ two coil configurations (coplanar and coaxial) there are only a maximum of three comparable frequencies per configuration, compared to 16 AeroTEM off-time and 12 AeroTEM on-time channels.

Figure 6 shows a comparison between the Dighem HEM system (900 Hz and 7200 Hz coplanar) and AeroTEM (Z-axis) from surveys flown in Raglan, in search of highly conductive Ni-Cu-PGM sulphide. In general, the AeroTEM peaks are sharper and better defined, in part due to the greater S/N ratio of the AeroTEM system over HEM, and also due to the modestly filtered AeroTEM data compared to HEM. The base levels are also better defined in the AeroTEM data. AeroTEM filtering is limited to spike removal and a 5-point smoothing filter. Clients are also given copies of the raw, unfiltered data.

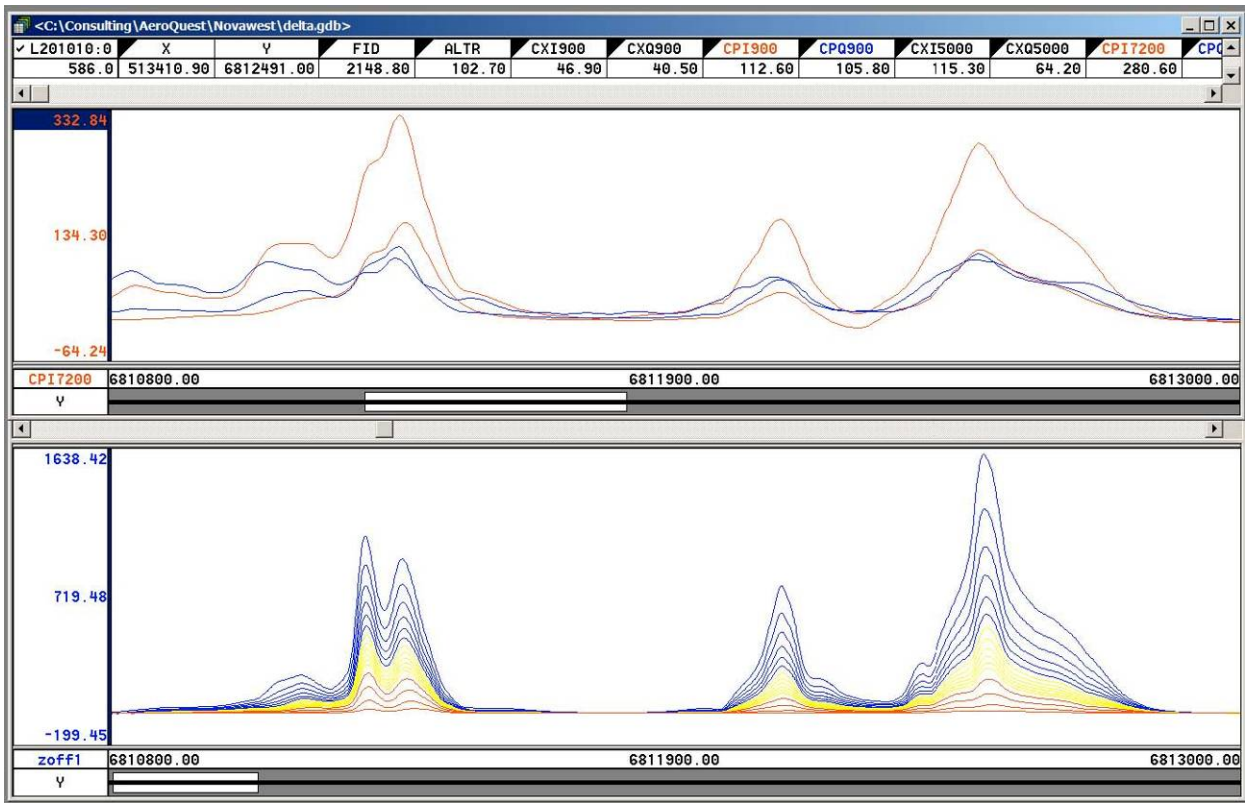

Figure 6. Comparison between Dighem HEM (upper) and AeroTEM (lower) surveys flown in the Raglan area. The AeroTEM responses appear to be more discrete, suggesting that the data is not as heavily filtered as the HEM data. The S/N advantage of AeroTEM over HEM is about 5:1.

Aeroquest Limited is grateful to the following companies for permission to publish some of the data from their respective surveys: Wolfden Resources, FNX Mining Company Inc, Canadian Royalties, Nova West Resources, Aurogin Resources, Spectrem Air. Permission does not imply an endorsement of the AeroTEM system by these companies.

APPENDIX 5: AEROTEM INSTRUMENTATION SPECIFICATION SHEET

AEROTEM Helicopter Electromagnetic System

System Characteristics

- Transmitter: Triangular Pulse Shape Base Frequency 90 Hz
- Tx On Time – 1,833 (90 Hz) µs
- Tx Off Time – 3,667 (90 Hz) µs
- Loop Diameter - 10 m
- Peak Current - 455 A
- Peak Moment – 178,600 NIA
- Typical Z Axis Noise at Survey Speed = 5 nT/s peak to peak
- Sling Weight: 1000 lb
- Length of Tow Cable: 48.8 m
- Bird Survey Height: 30 m nominal

Receiver

- Two Axis Receiver Coils (x, z) positioned inside the transmitter loop
- Selectable Time Delay to start of first channel 21.3 , 42.7, or 64.0 ms

Display & Acquisition

- AERODAS Digital recording at 200 samples per decay curve at a maximum of 180 decay curves per second (27.778 µs channel width)
- RMS Channel Widths: 52.9,132.3, 158.7, 158.7, 317.5, 634.9 µs
- Recording & Display Rate = 10 readings per second.
- On-board display - six channels Z-component and 1 X-component

System Considerations

Comparing a fixed-wing time domain transmitter with a typical moment of 500,000 NIA flying at an altitude of 120 m with a Helicopter TDEM at 30 m, notwithstanding the substantial moment loss in the airframe of the fixed wing, the same penetration by the lower flying helicopter system would only require a sixty-fourth of the moment. Clearly the AeroTEM system with nearly 183.131 NIA has more than sufficient moment. The airframe of the fixed wing presents a response to the towed bird, which requires dynamic compensation. This problem is non-existent for AeroTEM since transmitter and receiver positions are fixed. The AeroTEM system is completely portable, and can be assembled at the survey site within half a day.

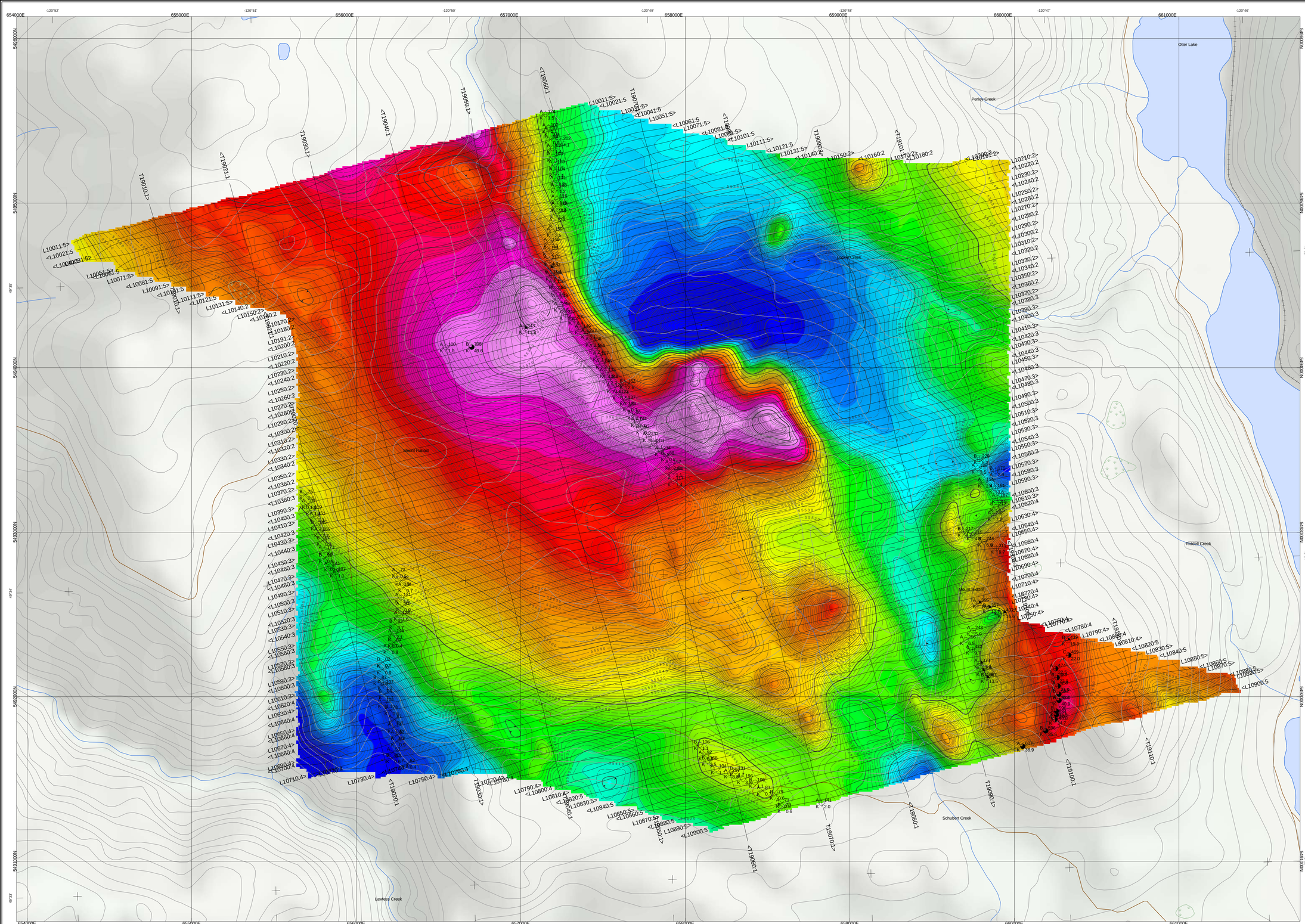

Grid North
NAD83-Zone10

The topographic data base was derived from 1:50000 NRC (Natural Resources Canada) NTDB data
Topo contours derived from NASA SRTM (Shuttle Radar Topography Mission) data
Inset data derived from Natural Resources Canada 'Atlas of Canada Base Maps'

This map accompanies the technical report entitled 'Report on a Helicopter-Borne Magnetic and Electromagnetic Survey, Princeton, BC', by Aeroquest Limited, February 2010

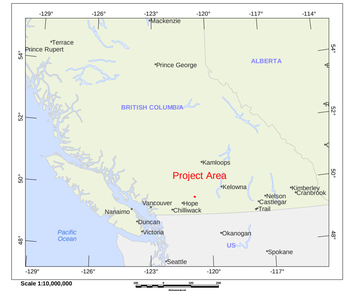

TMI nT	
55955.8	
55905.0	
55856.3	
55816.3	
55789.0	
55771.8	
55754.9	
55740.2	
55723.5	
55707.4	
55688.1	
55668.8	
55650.2	
55630.8	
55613.9	
55598.9	
55583.3	
55563.8	
55543.3	
55526.1	
55511.3	
55500.6	
55489.7	
55481.3	
55473.0	
55463.9	
55454.2	
55443.1	
55430.6	
55420.6	
55410.7	
55397.6	
55385.5	
55375.2	
55361.9	
55341.6	
55313.8	
55274.8	

Off-Time Anomaly Symbols

>50S	
35-50S	
20-35S	
10-20S	
5-10S	
1-5S	
<1S	

anomaly label — A 125 — decay constant (µs)
thick/thin source — K 36 — off-time conductance (S)

Rail	
Roads / Trails	
Wetland	
Lake and Streams	

Contour Interval

5nT
10nT
50nT
250nT

SURVEY SPECIFICATIONS:
- Survey flown: December 7-9, 2009
- Traverse/Tie line spacing: 50/500 metres
- Traverse/Tie line direction: (75°/255°)/(165°/345°)
- Nominal EM bird height: 30 metres
- Aircraft: Aerospatiale SA 315B (C-GLOV)

INSTRUMENTATION:
- Data acquisition: ADAS
- Magnetometer: Geometrics G-823A cesium vapour
  - Installation: Towed bird 33 m above EM bird
  - Sensitivity: .001 nanoTesla
- Electromagnetics: AeroTEM III System (MIKE)
  - Configuration: Towed bird

NAVIGATION:
- Navigation: Differential Global Positioning System (DGPS)
- Navigation equipment: AGNAV with MID-TECH RX400p receiver
- Radar Altimeter: Terra TRA3000/TRI-30

DATA PROCESSING
- Magnetics: diurnal, tieline and micro-leveling corrections

POSITIONING
- Datum: NAD83
  - Major Axis: 6378137.000
  - Eccentricity: 0.081819191

MAP PROJECTION
- Projection: Universal Transverse Mercator
- Central Meridian: 123°W (Zone 10)
- Central Scale Factor: 0.9996
- False Easting/Northing: 500,000m/0m

scale 1:10,000

200 0 200 400 600
(meters)
NAD83 / UTM zone 10N

Max Investments Inc. on behalf of Discovery Venures Inc.
Princeton, British Columbia

TOTAL MAGNETIC INTENSITY
Rabbitt Mine

NTS 092H10

AEROQUEST
7687 Bath Road, Mississauga, ON, CANADA L4T 3T1
Tel: (905) 672-9129 Fax: (905) 672-7083
www.aeroquest.ca

February 2010

TMI

TMI_10k_Rabbitt Mine.map, AQL Job no. 10007

654000E 655000E 656000E 657000E 658000E 659000E 660000E 661000E

549300N 549200N 549100N

-120°52' -120°51' -120°50' -120°49' -120°48' -120°47' -120°46'

49°35' 49°34' 49°33'

Otter Lake
Perley Creek
Locker Creek
Mount Rabbit
Riddell Creek
Schubert Creek
Lawless Creek

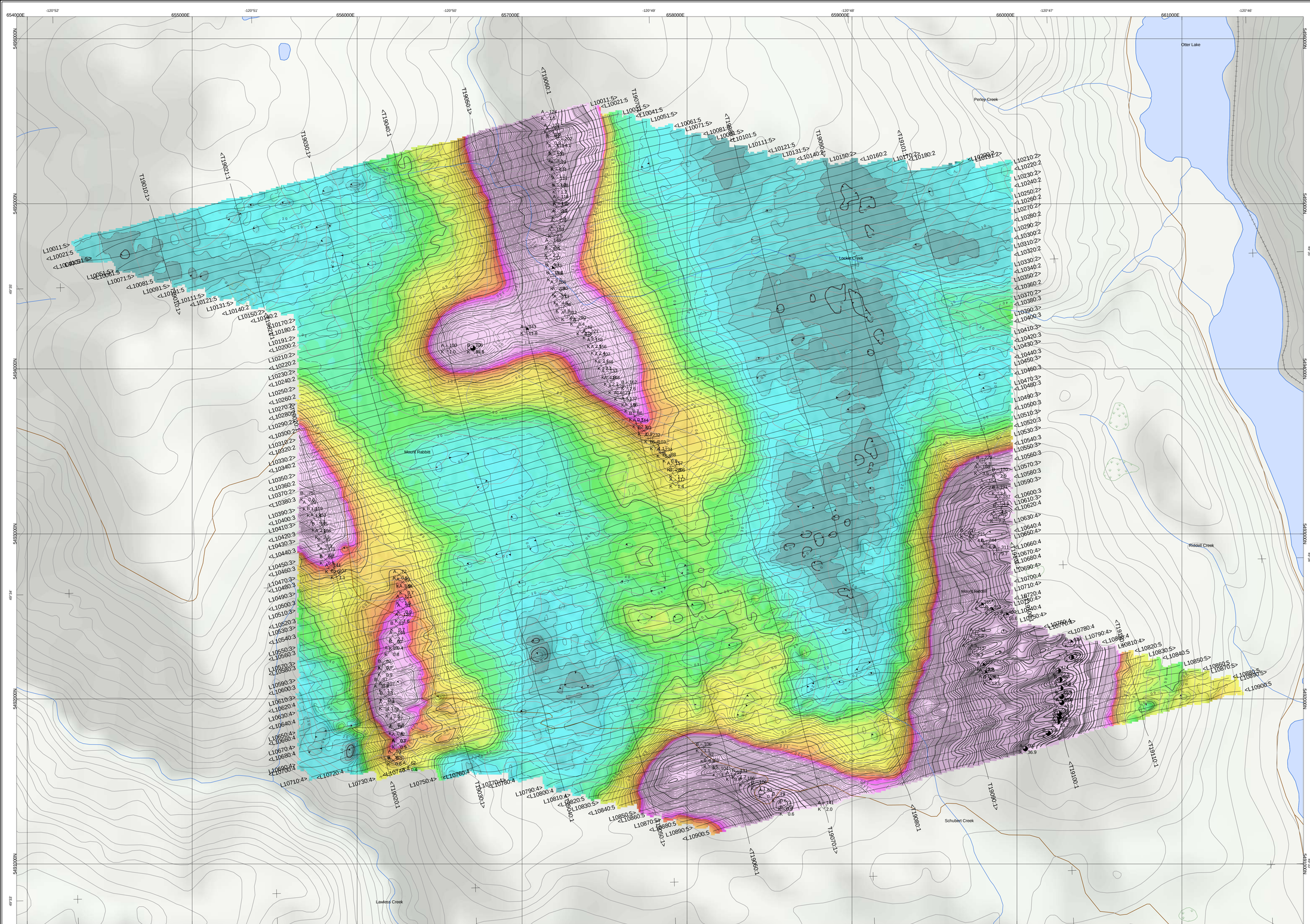

Grid North
NAD83-Zone10

The topographic data base was derived from 1:50000 NRC (Natural Resources Canada) NTDB data
Topo contours derived from NASA SRTM (Shuttle Radar Topography Mission) data
Inset data derived from Natural Resources Canada 'Atlas of Canada Base Maps'

This map accompanies the technical report entitled 'Report on a Helicopter-Borne Magnetic and Electromagnetic Survey, Princeton, BC', by Aeroquest Limited, February 2010

Off-Time Anomaly Symbols

>50S	
35-50S	
20-35S	
10-20S	
5-10S	
1-5S	
<1S	

anomaly label A 125 K 36 decay constant (µs)
thicK/thiN source off-time conductance (S)

Z1-OFF nT/s	
145	
140	
134	
129	
124	
119	
114	
109	
103	
98	
93	
88	
83	
78	
72	
67	
62	
57	
52	
47	
41	
36	
31	
26	
21	
16	
10	
5	

Contour Interval
5 nT/s
10 nT/s
50 nT/s
250 nT/s

Rail
Roads / Trails
Wetland
Lake and Streams

SURVEY SPECIFICATIONS:
- Survey flown: December 7-9, 2009
- Traverse/Tie line spacing: 50/500 metres
- Traverse/Tie line direction: (75°/255°)/(165°/345°)
- Nominal EM bird height: 30 metres
- Aircraft: Aerospatiale SA 315B (C-GLOV)

INSTRUMENTATION:
- Data acquisition: ADAS
- Magnetometer: Geometrics G-823A cesium vapour
  - Installation: Towed bird 33 m above EM bird
  - Sensitivity: .001 nanoTesla
- Electromagnetics: AeroTEM III System (MIKE)
  - Configuration: Towed bird

NAVIGATION:
- Navigation: Differential Global Positioning System (DGPS)
- Navigation equipment: AGNAV with MID-TECH RX400p receiver
- Radar Altimeter: Terra TRA3000/TRI-30

DATA PROCESSING
- Magnetics: diurnal, tieline and micro-leveling corrections

POSITIONING
- Datum: NAD83
  - Major Axis: 6378137.000
  - Eccentricity: 0.081819191

MAP PROJECTION
- Projection: Universal Transverse Mercator
- Central Meridian: 123°W (Zone 10)
- Central Scale Factor: 0.9996
- False Easting/Northing: 500,000m/0m

scale 1:10,000

200 0 200 400 600
Meters
NAD83 / UTM zone 10N

Max Investments Inc. on behalf of Discovery Venures Inc.
Princeton, British Columbia

AEROTEM Z1-OFF TIME
Time after TxOff 117µs
Rabbitt Mine

NTS 092H10

AEROQUEST
7687 Bath Road, Mississauga, ON, CANADA L4T 3T1
Tel. (905) 672-9129 Fax (905) 672-7083
www.aeroquest.ca

February 2010

Z1-OFF

Z1-OFF_10k_Rabbitt Mine.map, AQL Job no. 10007

654000E 655000E 656000E 657000E 658000E 659000E 660000E 661000E

-120°52' -120°51' -120°50' -120°49' -120°48' -120°47' -120°46'

5493000N 5492000N 5491000N

49°35' 49°34' 49°33'

Otter Lake

Perley Creek

Leaders Creek

Mount Rabbitt

Riddell Creek

Schubert Creek

Lawless Creek

EM_10k_Rabbitt More.map, AQL Job no. 10007

Grid North
NAD83-Zone10

The topographic data base was derived from 1:50000 NRC (Natural Resources Canada) NTDB data
Topo contours derived from NASA SRTM (Shuttle Radar Topography Mission) data
Inset data derived from Natural Resources Canada 'Atlas of Canada Base Maps'

This map accompanies the technical report entitled 'Report on a Helicopter-Borne Magnetic and Electromagnetic Survey, Princeton, BC', by Aeroquest Limited, February 2010

Off-Time Anomaly Symbols

>50S	●
35-50S	◕
20-35S	◑
10-20S	◔
5-10S	⊕
1-5S	◇
<1S	×

anomaly label A 125 K 36 — decay constant (µs)
thickK/thiN source — off-time conductance (S)

AeroTEM Profiles

positive excursion to top and right, 1mm=15nT/s

- Z3 Off-Time Channel 173 µs
- Z4 Off-Time Channel 200 µs
- Z5 Off-Time Channel 228 µs
- Z6 Off-Time Channel 284 µs
- Z7 Off-Time Channel 367 µs
- Z8 Off-Time Channel 450 µs
- Z9 Off-Time Channel 534 µs
- Z10 Off-Time Channel 645 µs
- Z11 Off-Time Channel 784 µs
- Z12 Off-Time Channel 950 µs
- Z13 Off-Time Channel 1186 µs

Rail
Roads / Trails
Wetland
Lake and Streams

SURVEY SPECIFICATIONS:
- Survey flown: December 7-9, 2009
- Traverse/Tie line spacing: 50/500 metres
- Traverse/Tie line direction: (75°/255°)/(165°/345°)
- Nominal EM bird height: 30 metres
- Aircraft: Aerospatiale SA 315B (C-GLOV)

INSTRUMENTATION:
- Data acquisition: ADAS
- Magnetometer, Geometrics G-823A cesium vapour
- Installation: Towed bird 33 m above EM bird
- Sensitivity: .001 nanoTesla
- Electromagnetics: AeroTEM III System (MIKE)
- Configuration: Towed bird

NAVIGATION:
- Navigation: Differential Global Positioning System (DGPS)
- Navigation equipment: AGNAV with MID-TECH RX400p receiver
- Radar Altimeter: Terra TRA3000/TRI-30

DATA PROCESSING
- Magnetics: diurnal, tieline and micro-leveling corrections

POSITIONING
- Datum: NAD83
  - Major Axis: 6378137.000
  - Eccentricity: 0.081819191

MAP PROJECTION
- Projection: Universal Transverse Mercator
- Central Meridian: 123°W (Zone 10)
- Central Scale Factor: 0.9996
- False Easting/Northing: 500,000m/0m

scale 1:10,000

200 0 200 400 600
(metres)
NAD83 / UTM zone 10N

Max Investments Inc. on behalf of Discovery Venures Inc.
Princeton, British Columbia

AEROTEM OFF-TIME PROFILES
Rabbitt Mine

NTS 092H10

AEROQUEST
7687 Bath Road, Mississauga, ON, CANADA L4T 3T1
Tel: (905) 672-9129 Fax: (905) 672-7083
www.aeroquest.ca

February 2010

EM

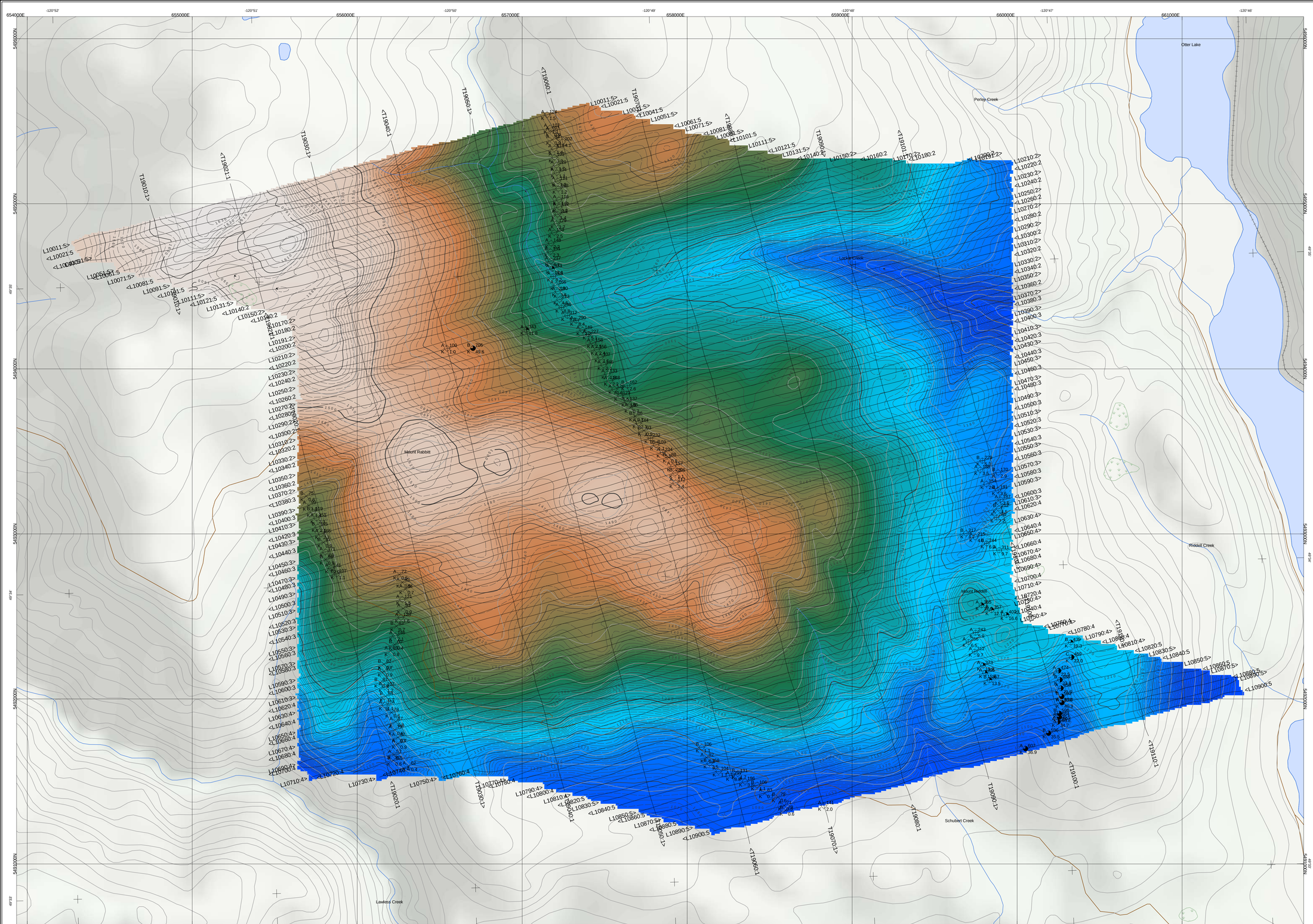

Grid North
NAD83-Zone10

The topographic data base was derived from 1:50000 NRC (Natural Resources Canada) NTDB data
Topo contours derived from NASA SRTM (Shuttle Radar Topography Mission) data
Inset data derived from Natural Resources Canada 'Atlas of Canada Base Maps'

This map accompanies the technical report entitled 'Report on a Helicopter-Borne Magnetic and Electromagnetic Survey, Princeton, BC', by Aeroquest Limited, February 2010

Off-Time Anomaly Symbols

- >50S .....
- 35-50S .....
- 20-35S .....
- 10-20S .....
- 5-10S .....
- 1-5S .....
- <1S .....

anomaly label: A 125 / K 36 — decay constant (µs) / thick/thN source / off-time conductance (S)

DTM metres: 1611, 1588, 1563, 1538, 1513, 1500, 1491, 1482, 1475, 1468, 1459, 1450, 1441, 1433, 1426, 1418, 1410, 1401, 1391, 1383, 1375, 1366, 1357, 1348, 1340, 1333, 1326, 1318, 1310, 1300, 1291, 1282, 1273, 1264, 1255, 1245, 1237, 1229, 1221, 1213, 1205, 1196, 1187, 1178, 1169, 1159, 1149, 1136, 1121, 1104, 1084, 1055

Contour Interval
- 5 m
- 10 m
- 50 m
- 250 m

- Rail
- Roads / Trails
- Wetland
- Lake and Streams

SURVEY SPECIFICATIONS:
- Survey flown: December 7-9, 2009
- Traverse/Tie line spacing: 50/500 metres
- Traverse/Tie line direction: (75°/255°)/(165°/345°)
- Nominal EM bird height: 30 metres
- Aircraft: Aerospatiale SA 315B (C-GLOV)

INSTRUMENTATION:
- Data acquisition: ADAS
- Magnetometer: Geometrics G-823A cesium vapour
  - Installation: Towed bird 33 m above EM bird
  - Sensitivity: .001 nanoTesla
- Electromagnetics: AeroTEM III System (MIKE)
  - Configuration: Towed bird

NAVIGATION:
- Navigation: Differential Global Positioning System (DGPS)
- Navigation equipment: AGNAV with MID-TECH RX400p receiver
- Radar Altimeter: Terra TRA3000/TRI-30

DATA PROCESSING
- Magnetics: diurnal, tieline and micro-leveling corrections

POSITIONING
- Datum: NAD83
  - Major Axis: 6378137.000
  - Eccentricity: 0.081819191

MAP PROJECTION
- Projection: Universal Transverse Mercator
- Central Meridian: 123°W (Zone 10)
- Central Scale Factor: 0.9996
- False Easting/Northing: 500,000m/0m

scale 1:10,000

200 0 200 400 600
(meters)
NAD83 / UTM zone 10N

Max Investments Inc. on behalf of Discovery Venures Inc.
Princeton, British Columbia

DIGITAL TERRAIN MODEL
Rabbitt Mine

NTS 092H10

AEROQUEST
7687 Bath Road, Mississauga, ON, CANADA L4T 3T1
Tel: (905) 672-9129 Fax: (905) 672-7083
www.aeroquest.ca

February 2010

DTM

DTM_10k_Rabbitt Mine.map, AQL Job no. 10007

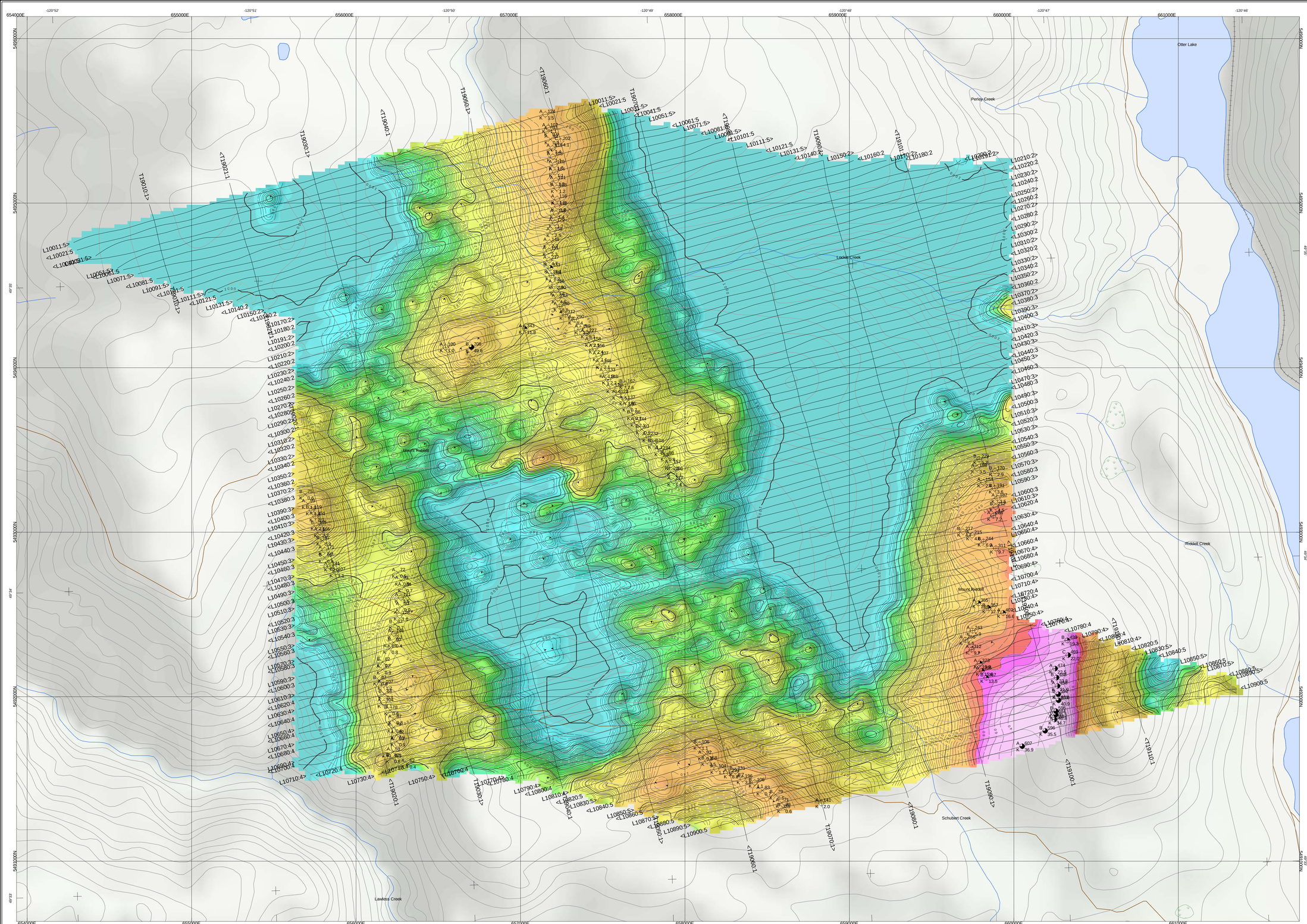

RES_10k_Rabbitt Mine.map, AQL Job no. 10007